

PREPARED FOR SUBMISSION TO JHEP

# Long Lived Light Scalars as Probe of Low Scale Seesaw Models

**P. S. Bhupal Dev,<sup>a</sup> Rabindra N. Mohapatra,<sup>b</sup> Yongchao Zhang<sup>c</sup>**

<sup>a</sup>*Department of Physics and McDonnell Center for the Space Sciences, Washington University, St. Louis, MO 63130, USA*

<sup>b</sup>*Maryland Center for Fundamental Physics, Department of Physics, University of Maryland, College Park, MD 20742, USA*

<sup>c</sup>*Service de Physique Théorique, Université Libre de Bruxelles, Boulevard du Triomphe, CP225, 1050 Brussels, Belgium*

*E-mail:* [bdev@wustl.edu](mailto:bdev@wustl.edu), [rmohapat@umd.edu](mailto:rmohapat@umd.edu), [yongchao.zhang@ulb.ac.be](mailto:yongchao.zhang@ulb.ac.be)

**ABSTRACT:** We point out that in generic TeV scale seesaw models for neutrino masses with local  $B - L$  symmetry breaking, there is a phenomenologically allowed range of parameters where the Higgs field responsible for  $B - L$  symmetry breaking leaves a physical real scalar field which could have a mass around GeV scale. This particle (denoted here by  $H_3$ ) is weakly mixed with the Standard Model Higgs field ( $h$ ) with mixing  $\theta_1 \lesssim m_{H_3}/m_h$  barring fine-tuned cancellation. When the  $B - L$  symmetry is embedded into the TeV scale left-right seesaw scenario, we show that these bounds on the  $h - H_3$  mixing  $\theta_1$  become further strengthened due to low energy flavor constraints, thus forcing the light  $H_3$  to be long lived. We discuss the production and decay of this new scalar field at the LHC and show that it leads to testable displaced vertex signals of collimated photon jets. We also study a simpler version of the model where the  $SU(2)_R$  breaking scale is much higher than  $U(1)_{B-L}$  which is at the TeV scale, in which case the production and decay of  $H_3$  proceed differently, but its long lifetime feature is still preserved. Thus, the long-lived light scalar particle provides a new way to probe TeV scale seesaw models for neutrino masses at colliders.

**KEYWORDS:** Neutrino Mass, Light Scalar, Large Hadron Collider

---

## Contents

<b>1</b>	<b>Introduction</b>	<b>2</b>
<b>2</b>	<b>Minimal left-right seesaw model</b>	<b>3</b>
<b>3</b>	<b>Light scalar in TeV-scale LR seesaw</b>	<b>4</b>
3.1	Parameters for a light scalar	5
3.2	Radiative corrections	6
3.3	Couplings of $H_3$	7
3.4	Decay lifetime and branching ratios	9
<b>4</b>	<b>Cosmological constraints</b>	<b>11</b>
<b>5</b>	<b>Laboratory Constraints</b>	<b>12</b>
5.1	$K$ and $B$ meson oscillations	12
5.2	Meson decay	14
5.2.1	$K$ meson decay	17
5.2.2	$B$ meson decay	18
5.2.3	Beam-dump experiments	22
5.3	SM Higgs, $Z$ and top decays	23
<b>6</b>	<b>Production and displaced vertex searches at colliders</b>	<b>25</b>
6.1	Production cross section	25
6.2	Prospects at the LHC	26
6.3	Prospects at future 100 TeV collider	28
6.4	Probing the LR seesaw model	29
<b>7</b>	<b>Light neutral scalar in <math>U(1)_{B-L}</math> model</b>	<b>31</b>
7.1	Couplings and decay	32
7.2	Meson limits	32
7.3	Production and LLP searches	33
<b>8</b>	<b>Discussions and Conclusion</b>	<b>34</b>
<b>A</b>	<b>Partial decay widths of <math>H_3</math></b>	<b>35</b>
<b>B</b>	<b>Rare <math>Z</math> decay <math>Z \rightarrow \gamma H_3</math></b>	<b>37</b>
<b>C</b>	<b>Light RH neutrinos in the LR seesaw model</b>	<b>37</b>

---

# 1 Introduction

Seesaw mechanism seems to provide a very simple and elegant way to understand the smallness of neutrino masses [1–5]. Two key ingredients of this mechanism are: (i) addition of the right-handed neutrinos (RHN) to the Standard Model (SM), and (ii) a large Majorana mass for the RHNs which breaks the accidental  $B - L$  symmetry of the SM. There exist a large class of ultraviolet(UV)-complete seesaw models which necessarily employ local  $B - L$  symmetry. It will therefore be an important step to find experimental evidence for this symmetry and its breaking. If the local  $B - L$  is broken by a Higgs field that carries this quantum number, there will be a remnant neutral scalar field, denoted here by  $H_3$  (for reasons explained below), analogous to the Higgs boson  $h$  of the SM. So looking for signatures of  $H_3$  can provide invaluable clues to the nature of the new physics associated with neutrino mass generation. Clearly, such a search is realistic only if the  $B - L$  symmetry breaking scale is in the multi-TeV range. The mass and couplings of the new Higgs field are still unrestricted to a large extent, mainly because it communicates to the SM sector only through its mixing with the SM Higgs and via the heavy gauge boson interactions. We will focus on the more interesting regime with  $m_{H_3} \ll m_h$  in which case, the  $H_3 - h$  mixing angle  $\theta_1 \lesssim m_{H_3}/m_h \simeq 8 \times 10^{-3} (m_{H_3}/\text{GeV})$  from considerations of fine tuning.

Smaller values of  $\theta_1$  can be analyzed as part of the allowed parameter range of generic  $B - L$  models. However, as we show here, this is naturally dictated to us from low energy flavor constraints once the  $B - L$  symmetry is embedded into the minimal TeV-scale left-right (LR) symmetric model [6–8], which is one of the most well-motivated UV-complete seesaw scenarios. This leads to the  $H_3$  particle being necessarily long-lived, with interesting displaced vertex signals at the Large Hadron Collider (LHC), as pointed out recently by us [9]. In this paper, we elaborate on the details of this scenario, including an in-depth discussion of all relevant high and low-energy constraints on the model parameter space, the production and decay of the new Higgs boson at the LHC and future colliders, as well as the experimental prospects of observing the displaced vertex signal. We will discuss two classes of UV-complete theories, based on (i) the full LR gauge group  $SU(2)_L \times SU(2)_R \times U(1)_{B-L}$ , and (ii) a simpler  $B - L$  model with  $SU(2)_L \times U(1)_{I_{3R}} \times U(1)_{B-L}$  local symmetry. The latter can be thought of as an “effective” theory of the LR model, where the  $SU(2)_R$  symmetry breaking scale is much higher than the  $U(1)_{B-L}$ -breaking which is assumed to be at the TeV-scale, but we believe that our results are applicable to a wider class of  $Z'$ -models.

The rest of the paper is organized as follows: in Section 2, we briefly review the minimal LR seesaw model and set up our notation. In Section 3, we present the arguments for the light  $B - L$  breaking Higgs being weakly mixed with the SM Higgs  $h$  and the heavy CP-even Higgs  $H_1$ , and study its decay lifetime and branching ratios. In Section 4, we derive a lower limit on the light scalar  $H_3$  mass from cosmological considerations at the nucleosynthesis epoch. In Section 5, we present an in-depth analysis of all available laboratory constraints on the light scalar parameter space. In Section 6, we discuss the production of  $H_3$  at hadron colliders and its detection prospects at the LHC, as well as in future colliders. In Section 7, we analyze the LLP prospects of a simpler  $U(1)_{B-L}$  model. Our conclusions are given in Section 8. In Appendix A, we collect the two-body partial decay widths of  $H_3$

in the LR model, and in Appendix B, the partial decay width of the loop-induced process  $Z \rightarrow H_3 \gamma$ . Finally, in Appendix C, we study the LLP sensitivity of light right-handed neutrinos in the LR model at the LHC.

## 2 Minimal left-right seesaw model

For completeness and to set up our notation, we briefly review the minimal LR model [6–8] in this section, based on the gauge group  $SU(3)_c \times SU(2)_L \times SU(2)_R \times U(1)_{B-L}$ . The quarks and leptons are assigned to the following irreducible representations:

$$Q_{L,i} = \begin{pmatrix} u_L \\ d_L \end{pmatrix}_i : \left( \mathbf{3}, \mathbf{2}, \mathbf{1}, \frac{1}{3} \right), \quad Q_{R,i} = \begin{pmatrix} u_R \\ d_R \end{pmatrix}_i : \left( \mathbf{3}, \mathbf{1}, \mathbf{2}, \frac{1}{3} \right), \quad (2.1)$$

$$\psi_{L,i} = \begin{pmatrix} \nu_L \\ e_L \end{pmatrix}_i : (\mathbf{1}, \mathbf{2}, \mathbf{1}, -1), \quad \psi_{R,i} = \begin{pmatrix} N_R \\ e_R \end{pmatrix}_i : (\mathbf{1}, \mathbf{1}, \mathbf{2}, -1), \quad (2.2)$$

where  $i = 1, 2, 3$  represents the family index, and the subscripts  $L, R$  denote the left- and right-handed chiral projection operators  $P_{L,R} = (1 \mp \gamma_5)/2$ , respectively. There are different ways to break the  $SU(2)_R \times U(1)_{B-L}$  gauge symmetry and to understand the small neutrino masses in this model, depending on the choice of the Higgs fields. One of the simplest choices is to introduce bi-doublet and triplet scalars

$$\Phi = \begin{pmatrix} \phi_1^0 & \phi_2^+ \\ \phi_1^- & \phi_2^0 \end{pmatrix} : (\mathbf{1}, \mathbf{2}, \mathbf{2}, 0), \quad \Delta_R = \begin{pmatrix} \Delta_R^+/\sqrt{2} & \Delta_R^{++} \\ \Delta_R^0 & -\Delta_R^+/\sqrt{2} \end{pmatrix} : (\mathbf{1}, \mathbf{1}, \mathbf{3}, 2), \quad (2.3)$$

respectively, with the neutral components of the above fields acquiring non-zero vacuum expectation values (VEV):

$$\langle \Delta_R^0 \rangle = v_R, \quad \langle \phi_1^0 \rangle = \kappa, \quad \langle \phi_2^0 \rangle = \kappa', \quad (2.4)$$

with the electroweak (EW) VEV given by  $v_{EW} = \sqrt{\kappa^2 + \kappa'^2} \simeq 174$  GeV. We assume the  $v_R$  scale to be in the multi-TeV range for phenomenological purposes. The scalar sector is chosen to be parity asymmetric, without the left-handed triplet counterpart  $\Delta_L$ , since we assume that parity has been broken at a much higher scale than  $SU(2)_R$  [10]. This makes it simpler to analyze and present our main results, although our conclusions remain unchanged in the fully parity symmetric version being a TeV scale theory.

The fermion masses can be understood from the Yukawa Lagrangian:

$$\begin{aligned} \mathcal{L}_Y = & h_{q,ij} \bar{Q}_{L,i} \Phi Q_{R,j} + \tilde{h}_{q,ij} \bar{Q}_{L,i} \tilde{\Phi} Q_{R,j} + h_{\ell,ij} \bar{\psi}_{L,i} \Phi \psi_{R,j} + \tilde{h}_{\ell,ij} \bar{\psi}_{L,i} \tilde{\Phi} \psi_{R,j} \\ & + f_{ij} \psi_{R,i}^T C i \sigma_2 \Delta_R \psi_{R,j} + \text{H.c.}, \end{aligned} \quad (2.5)$$

where  $\tilde{\Phi} = i \sigma_2 \Phi^*$  (with  $\sigma_2$  being the second Pauli matrix) and  $C$  stands for charge conjugation. The standard type-I seesaw mass matrix for neutrinos follows from the leptonic part of the above couplings after symmetry breaking. The triplet VEV  $v_R$  breaks lepton number and provides the Majorana mass for the heavy RHNs which goes into the seesaw matrix [2].

### 3 Light scalar in TeV-scale LR seesaw

In this section, we analyze the TeV-scale LR seesaw parameter space for a light scalar with mass in the (sub) GeV range and its couplings to determine the decay branching ratios and lifetime.

The most general scalar potential for this model reads as follows:

$$\begin{aligned}
\mathcal{V} = & -\mu_1^2 \text{Tr}(\Phi^\dagger \Phi) - \mu_2^2 \left[ \text{Tr}(\tilde{\Phi} \Phi^\dagger) + \text{Tr}(\tilde{\Phi}^\dagger \Phi) \right] - \mu_3^2 \text{Tr}(\Delta_R \Delta_R^\dagger) \\
& + \lambda_1 \left[ \text{Tr}(\Phi^\dagger \Phi) \right]^2 + \lambda_2 \left\{ \left[ \text{Tr}(\tilde{\Phi} \Phi^\dagger) \right]^2 + \left[ \text{Tr}(\tilde{\Phi}^\dagger \Phi) \right]^2 \right\} \\
& + \lambda_3 \text{Tr}(\tilde{\Phi} \Phi^\dagger) \text{Tr}(\tilde{\Phi}^\dagger \Phi) + \lambda_4 \text{Tr}(\Phi^\dagger \Phi) \left[ \text{Tr}(\tilde{\Phi} \Phi^\dagger) + \text{Tr}(\tilde{\Phi}^\dagger \Phi) \right] \\
& + \rho_1 \left[ \text{Tr}(\Delta_R \Delta_R^\dagger) \right]^2 + \rho_2 \text{Tr}(\Delta_R \Delta_R) \text{Tr}(\Delta_R^\dagger \Delta_R^\dagger) \\
& + \alpha_1 \text{Tr}(\Phi^\dagger \Phi) \text{Tr}(\Delta_R \Delta_R^\dagger) + \left[ \alpha_2 e^{i\delta_2} \text{Tr}(\tilde{\Phi} \Phi^\dagger) \text{Tr}(\Delta_R \Delta_R^\dagger) + \text{H.c.} \right] + \alpha_3 \text{Tr}(\Phi^\dagger \Phi \Delta_R \Delta_R^\dagger).
\end{aligned} \tag{3.1}$$

All the 12 parameters  $\mu_{1,2,3}^2$ ,  $\lambda_{1,2,3,4}$ ,  $\rho_{1,2}$ ,  $\alpha_{1,2,3}$  are chosen to be real, with an appropriate redefinition of the fields, and the only CP-violating phase  $\delta_2$  is associated with the coupling  $\alpha_2$ , as explicitly shown in Eq. (3.1). There are 14 scalar degrees of freedom, six of which are Goldstone modes eaten by the  $W^\pm, W_R^\pm, Z, Z_R$  gauge bosons, thus leaving 8 physical Higgs bosons, denoted by  $h, H_1, A_1, H_3, H_1^\pm$  and  $H_2^{\pm\pm}$ . The full scalar potential for this class of LR seesaw models was analyzed in detail in Refs. [11–13] and here we present only the results relevant for our purpose.

We work in the natural parameter space, where the following parameters are small:

$$\xi \equiv \kappa'/\kappa = \frac{m_b}{m_t} \ll 1, \quad \epsilon \equiv \kappa'/v_R \ll v_{EW}/v_R \ll 1, \tag{3.2}$$

and also assume that there is no CP-violation in the scalar sector, i.e. the CP-violating phase  $\delta_2$  is zero. There are 6 degrees of freedom in the neutral scalar sector: three dominantly CP-even and the other three CP-odd. This includes the two Goldstone modes eaten by the neutral  $Z$  and  $Z_R$  gauge bosons. In the CP-even sector of neutral scalars, after applying the minimization conditions with respect to the three VEVs  $\kappa, \kappa', v_R$  and the phase  $\delta_2$  associated with the VEV  $\kappa'$ , we obtain the squared mass matrices in the basis of  $\{\phi_1^{0\text{Re}}, \phi_2^{0\text{Re}}, \Delta_R^{0\text{Re}}\}$  at the zeroth, first and second order of the small parameters  $\xi$  and  $\epsilon$  defined in Eq. (3.2) (setting the phase  $\delta_2$  to be zero), respectively,

$$(\mathcal{M}_0^2)^{(0)} = v_R^2 \begin{pmatrix} 0 & 0 & 0 \\ 0 & \alpha_3 & 0 \\ 0 & 0 & 4\rho_1 \end{pmatrix}, \tag{3.3}$$

$$(\mathcal{M}_0^2)^{(1)} = v_R^2 \begin{pmatrix} 0 & -\alpha_3 \xi & 2\alpha_1 \epsilon \\ -\alpha_3 \xi & 0 & 4\alpha_2 \epsilon \\ 2\alpha_1 \epsilon & 4\alpha_2 \epsilon & 0 \end{pmatrix}, \tag{3.4}$$

$$(\mathcal{M}_0^2)^{(2)} = v_R^2 \begin{pmatrix} 4\lambda_1 \epsilon^2 + \alpha_3 \xi^2 & 4\lambda_4 \epsilon^2 & 4\alpha_2 \epsilon \xi \\ 4\lambda_4 \epsilon^2 & 4(2\lambda_2 + \lambda_3) \epsilon^2 + \alpha_3 \xi^2 & 2(\alpha_1 + \alpha_3) \epsilon \xi \\ 4\alpha_2 \epsilon \xi & 2(\alpha_1 + \alpha_3) \epsilon \xi & 0 \end{pmatrix}. \tag{3.5}$$

In the limit of  $\xi \ll 1$ , one of the scalars, predominantly from  $\phi_2^{0\text{Re}}$  is heavy, with mass at the  $v_R$  scale  $\sqrt{\alpha_3}v_R$  and decouples from the lower energy SM sector, thus leading to a reduced scalar mass matrix involving only  $\phi_1^{0\text{Re}}$  and  $\Delta_R^{0\text{Re}}$ . If the quartic coupling  $\rho_1$  is large, say of order one, then  $\Delta_R^{0\text{Re}}$  (denoted here by  $H_3$ ) will also be heavy, close to the  $v_R$  scale, and its mixing with the SM Higgs boson  $h$  will be given by  $\theta_1 \simeq \frac{\alpha_1 v_{\text{EW}}}{\rho_1 v_R}$ . However, there exists another possibility, mainly motivated by the lack of any direct experimental constraints on its mass, as well as supported by arguments based on radiative stability (see Section 3.2), where  $H_3$  could also be very light, and in particular, lighter than the SM Higgs boson. This happens when  $\rho_1 \ll 1$ , in which case, the sub-matrix in the basis of  $\{\phi_1^{0\text{Re}}, \Delta_R^{0\text{Re}}\}$  is given by

$$\mathcal{M}_0^2 \simeq \begin{pmatrix} 4\lambda_1 \epsilon^2 & 2\alpha_1 \epsilon \\ 2\alpha_1 \epsilon & 4\rho_1 \end{pmatrix} v_R^2. \quad (3.6)$$

In the limit of  $m_{H_3}^2 \ll m_h^2$ , Eq. (3.6) can be diagonalized in a seesaw-like approximation, and the two scalar masses are respectively given by

$$m_h^2 \simeq 4\lambda_1 \epsilon^2 v_R^2 = 4\lambda_1 v_{\text{EW}}^2, \quad (3.7)$$

$$m_{H_3}^2 \simeq 4\rho_1 v_R^2 - \sin^2 \theta_1 m_h^2, \quad (3.8)$$

with the mixing angle

$$\sin \theta_1 \simeq \frac{\alpha_1}{2\lambda_1 \epsilon} = \frac{\alpha_1}{2\lambda_1} \frac{v_R}{v_{\text{EW}}}. \quad (3.9)$$

Note that the mixing has an inverted dependence on the VEV ratio  $(v_{\text{EW}}/v_R)^{-1}$ , compared to the case where  $m_{H_3} \gg m_h$ . This restricts the parameter  $\alpha_1$  to be appropriately small in order to ensure that  $\sin \theta_1 \leq 1$ , as we show below.

### 3.1 Parameters for a light scalar

The question that we address in this subsection is whether there is a range of parameters in the model where  $H_3$  could be light, i.e. in the (sub)-GeV range, which has important phenomenological ramifications. From Eq. (3.8), it is clear that the lightness of  $H_3$  depends on how small the values of  $\rho_1$  and  $\alpha_1$  can be:

$$m_{H_3}^2 \simeq \left(4\rho_1 - \frac{\alpha_1^2}{\lambda_1}\right) v_R^2. \quad (3.10)$$

The exact dependence of  $m_{H_3}$  on the parameters  $\rho_1$  and  $\alpha_1$  is shown in Figure 1 for a representative value of  $v_R = 5$  TeV, which is close to the smallest possible value allowed by the current direct [14–16] and indirect [17] constraints on the  $W_R$  mass (with appropriate scaling for  $g_R \neq g_L$ , where  $g_{L,R}$  are the  $SU(2)_{L,R}$  gauge couplings). We see that for  $\rho_1 \sim 10^{-8}$  and  $\alpha_1 \lesssim 10^{-5}$ , we get  $m_{H_3} \sim \mathcal{O}(\text{GeV})$ , which is the region of great interest for long-lived particle (LLP) searches, as we will see below. For a small mixing  $\sin \theta_1$ , the  $H_3$  mass is determined completely by  $\rho_1$  which is required to be very small for light  $H_3$ . However, when the mixing is sizable, i.e.  $\alpha_1$  is comparatively large, there can be large cancellation between the two terms in Eq. (3.8).

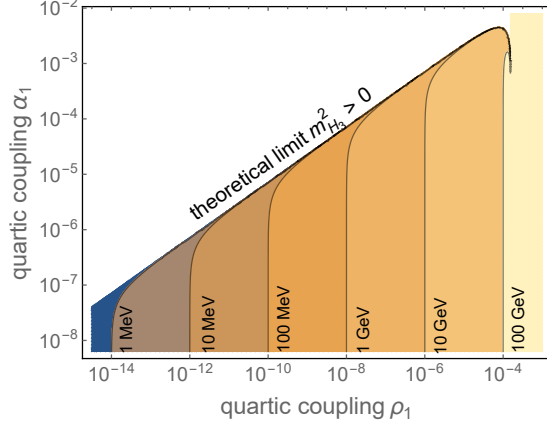


**Figure 1.** Contours of  $m_{H_3}$  as a function of the quartic coupling parameters  $\rho_1$  and  $\alpha_1$  defined in the scalar potential (3.1). Here we have set the RH triplet VEV  $v_R = 5$  TeV.

### 3.2 Radiative corrections

In this subsection, we consider the one-loop corrections to the  $H_3$  mass to see whether  $m_{H_3} \sim \mathcal{O}(\text{GeV})$  is radiatively stable. The one-loop renormalization group (RG) running of the gauge, quartic and Yukawa couplings in the LR model has been considered in Refs. [18–20]. Due to the large number of parameters in the scalar potential, some of the couplings would easily become non-perturbative before reaching up to the GUT or Planck scale, especially when the RH scale  $v_R$  is relatively low [13]. There are also stability and perturbativity constraints on some of the quartic couplings [21], but the mass of  $H_3$ , which is proportional to  $\sqrt{\rho_1}$  at the leading order at tree level [cf. Eq. (3.10)], is not limited by these arguments. Moreover, even if the gauge symmetry  $SU(2)_R$  is restored at the few-TeV scale, the LR model is far from being a UV-complete theory up to the GUT scale, and more fields have to be introduced at higher energy scales, which hardly leave any imprints at the TeV scale. Our aim here is not to analyze the ultimate UV-complete theory with parity, rather we remain at the TeV-scale, and using the Coleman-Weinberg effective potential approach [22], check how the mass of  $H_3$  would be affected by interacting with other particles in the TeV-scale LR model at the one-loop level.

Our considerations are similar to what happens to the SM Higgs mass. It is well known that if we neglect the one-loop fermion contributions to the Coleman-Weinberg effective potential, there would be a lower limit of order of 5 GeV on the Higgs boson mass [23, 24]. However, this bound goes away once the large top-quark Yukawa coupling is included. This approach for the LR models for the case of doublet Higgs but without singlet fermions was carried out in Ref. [25], where a lower bound on the heavy neutral Higgs of the order of 900 GeV was obtained. The crucial difference in our model is the fermion contribution, which enables us to avoid this lower bound on  $m_{H_3}$ .

In the Coleman-Weinberg effective potential, we find that the dominant one-loop corrections to  $m_{H_3}^2$  arise from its gauge interaction with the heavy  $W_R$ ,  $Z_R$  RH gauge bosons, the Yukawa interaction with the RHNs, and the interactions with the heavy scalars  $H_1$ ,  $A_1$ ,  $H_1^\pm$  and  $H_2^{\pm\pm}$ . All the interactions with the SM fields are suppressed by the small

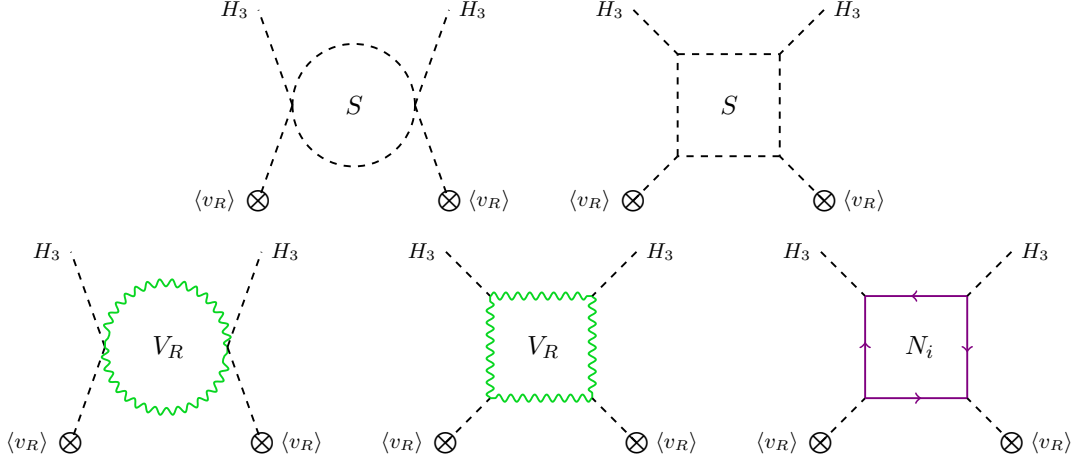


**Figure 2.** Dominant loop corrections to  $m_{H_3}^2$  from interacting with the heavy scalars  $S$  ( $H_1$ ,  $A_1$ ,  $H_1^\pm$ ,  $H_2^{\pm\pm}$ ), the heavy gauge bosons  $V_R$  ( $W_R$ ,  $Z_R$ ) and the heavy RHNs  $N_i$ .

mixing angles. The Feynman diagrams of loop corrections to  $m_{H_3}^2$  from the heavy particle loops are collected in Figure 2, which sum up to

$$(m_{H_3}^2)^{\text{loop}} \simeq \frac{3}{2\pi^2} \left[ \frac{1}{3}\alpha_3^2 + \frac{8}{3}\rho_2^2 - 8f^4 + \frac{1}{2}g_R^4 + (g_R^2 + g_{BL}^2)^2 \right] v_R^2, \quad (3.11)$$

where  $g_{BL}$  is the  $SU(2)_R$  and  $U(1)_{B-L}$  gauge coupling strength,  $f$  is the RHN Yukawa coupling as defined in Eq. (2.5), and  $\alpha_3$  and  $\rho_2$  are the scalar quartic couplings defined in Eq. (3.1). Without any tuning of the scalar, gauge and Yukawa couplings, the loop correction to  $m_{H_3}$  is expected to be of order  $v_R/4\pi$ . In the above expression, we have kept only the contribution of the scalar coupling  $\alpha_3$  since that is the only coupling which is expected to be of order one to satisfy the flavor changing neutral current (FCNC) constraints on Higgs mass ( $\text{Re } \phi_2^0$ ), as we will discuss below in Section 5. However, the important point to note here is that with the minus sign for the  $f$  contribution in Eq. (3.11), the bosonic and fermionic contributions can be made to cancel each other keeping  $H_3$  mass light even in the presence of radiative corrections. With a tuning of order  $\text{GeV}/\frac{v_R}{4\pi} \sim 10^{-2}$  (with  $v_R$  at the TeV-scale) for the parameters in Eq. (3.11), we could easily obtain a light scalar  $H_3$  at or below the GeV scale.

### 3.3 Couplings of $H_3$

In order to study the collider phenomenology of light  $H_3$ , it is essential to delineate its couplings to various particles in the theory. In the limit of zero CP phase  $\delta_2$  in Eq. (3.1),  $H_3$  could only mix with the scalars  $h$  and  $H_1$ :

$$\begin{pmatrix} h \\ H_1 \\ H_3 \end{pmatrix} = \begin{pmatrix} 1 - \frac{1}{2}\xi^2 & \xi & -\sin\theta_1 \\ -\xi & 1 - \frac{1}{2}\xi^2 & -\sin\theta_2 \\ \sin\theta_1 & \sin\theta_2 & 1 \end{pmatrix} \begin{pmatrix} \phi_1^{0\text{Re}} \\ \phi_2^{0\text{Re}} \\ \Delta_R^{0\text{Re}} \end{pmatrix}, \quad (3.12)$$

**Table 1.** The couplings of the light scalar  $H_3$ , up to the leading order in  $\epsilon$  and  $\xi$ .

couplings	values
$H_3 h h$	$\frac{1}{\sqrt{2}} \alpha_1 v_R$
$h H_3 H_3$	$-\sqrt{2} \alpha_1 v_{EW}$
$H_3 h H_1^0$	$2\sqrt{2} \alpha_2 v_R$
$H_3 H_1^0 H_1^0$	$\frac{1}{\sqrt{2}} \alpha_3 v_R$
$H_3 A_1^0 A_1^0$	$\frac{1}{\sqrt{2}} \alpha_3 v_R$
$H_3 H_1^+ H_1^-$	$\sqrt{2} \alpha_3 v_R$
$H_3 H_2^{++} H_2^{--}$	$2\sqrt{2} (\rho_1 + 2\rho_2) v_R$
$H_3 \bar{u} u$	$\frac{1}{\sqrt{2}} \hat{Y}_U \sin \tilde{\theta}_1 - \frac{1}{\sqrt{2}} \left( V_L \hat{Y}_D V_R^\dagger \right) \sin \tilde{\theta}_2$
$H_3 \bar{d} d$	$\frac{1}{\sqrt{2}} \hat{Y}_D \sin \tilde{\theta}_1 - \frac{1}{\sqrt{2}} \left( V_L^\dagger \hat{Y}_U V_R \right) \sin \tilde{\theta}_2$
$H_3 \bar{e} e$	$\frac{1}{\sqrt{2}} \hat{Y}_E \sin \tilde{\theta}_1 - \frac{1}{\sqrt{2}} Y_{\nu N} \sin \tilde{\theta}_2$
$H_3 N N$	$\frac{m_N}{\sqrt{2} v_R}$
$H_3 W^+ W^-$	$\frac{1}{\sqrt{2}} g_L^2 \sin \theta_1 v_{EW} + \sqrt{2} g_R^2 \sin^2 \zeta_W v_R$
$H_3 W^+ W_R^-$	$\sqrt{2} g_R^2 \sin \zeta_W v_R$
$H_3 W_R^+ W_R^-$	$\sqrt{2} g_R^2 v_R$
$H_3 Z Z$	$\frac{g_L^2 \sin \theta_1 v_{EW}}{2\sqrt{2} \cos^2 \theta_w} + \frac{\sqrt{2} g_R^2 \sin^2 \zeta_Z v_R}{\cos^2 \phi}$
$H_3 Z Z_R$	$-\frac{g_L g_R \sin \theta_1 \cos \phi v_{EW}}{\sqrt{2} \cos \theta_w} + \frac{2\sqrt{2} g_R^2 \sin \zeta_Z v_R}{\cos^2 \phi}$
$H_3 Z_R Z_R$	$\frac{\sqrt{2} g_R^2 v_R}{\cos^2 \phi}$
$H_3 H_1^+ W^-$	$\frac{1}{2} g_L (\sin \theta_2 - \sin \theta_1 \xi)$
$H_3 H_1^+ W_R^-$	$\frac{1}{2} g_R \epsilon$
$H_3 A_1 Z$	$-\frac{i g_L (\sin \theta_2 - \sin \theta_1 \xi)}{2 \cos \theta_w}$
$H_3 A_1 Z_R$	$\frac{i}{2} g_R (\sin \theta_2 - \sin \theta_1 \xi) \cos \phi$

where  $\sin \theta_1$  is the  $h - H_3$  mixing already defined in Eq. (3.9) and

$$\sin \theta_2 \simeq \frac{4\alpha_2 \epsilon}{\alpha_3} = \frac{4\alpha_2}{\alpha_3} \frac{v_{EW}}{v_R}. \quad (3.13)$$

is the mixing between  $H_3$  and  $H_1$ . Both  $\theta_1$  and  $\theta_2$  are expected to be small for a GeV-scale  $H_3$ . The “effective” mixing angles of  $H_3$  responsible for the flavor conserving and violating couplings to the SM quarks and charged leptons can be defined as

$$\sin \tilde{\theta}_1 \equiv \sin \theta_1 + \xi \sin \theta_2, \quad (3.14)$$

$$\sin \tilde{\theta}_2 \equiv \sin \theta_2 + \xi \sin \theta_1, \quad (3.15)$$

which will be used in our subsequent discussion.

For completeness we collect all the coupling of light  $H_3$  in the minimal LR models in Table 1, which is based on the calculation of Ref. [12] and up to the leading order in the small parameters  $\xi$  and  $\epsilon$  defined in Eq. (3.2). Here the RH gauge mixing  $\phi$  is defined as

$\tan \phi \equiv g_{BL}/g_R$ , and the  $W - W_R$  and  $Z - Z_R$  mixings are respectively given by

$$\tan \zeta_W \simeq -\frac{2g_R \xi}{g_L} \left( \frac{m_W}{m_{W_R}} \right)^2, \quad (3.16)$$

$$\tan \zeta_Z \simeq \left[ \frac{g_R^2}{g_L^2} - \left( 1 + \frac{g_R^2}{g_L^2} \right) \sin^2 \theta_w \right]^{1/2} \left( \frac{m_Z}{m_{Z_R}} \right)^2, \quad (3.17)$$

where  $\theta_w$  is the weak mixing angle.

In Table 1, the couplings to the charged leptons depend on the neutrino sector via the Dirac coupling matrix  $Y_{\nu N} = m_D/v_{EW}$ , which can be parameterized through the Casas-Ibarra form [26]

$$m_D = i m_N^{1/2} O m_\nu^{1/2} \quad (3.18)$$

with  $O$  an arbitrary complex orthogonal matrix,  $m_\nu$  and  $m_N$  are the light neutrino and RHN mass matrix, respectively.

### 3.4 Decay lifetime and branching ratios

Through the mixing with the SM Higgs and the heavy scalar  $H_1$  via respectively the mixing angles  $\sin \theta_1$  and  $\sin \theta_2$  in Eq. (3.9) and (3.13), a light  $H_3$  could decay at tree level into the SM fermions, cf. the Yukawa couplings in Table 1. Note that the couplings to quarks could be flavor-changing, depending on the magnitude of effective mixing angle  $\sin \tilde{\theta}_2$ , while the lepton flavor violating (LFV) couplings are proportional to the Dirac coupling  $Y_{\nu N}$  and  $\sin \tilde{\theta}_2$ . At the one-loop level, the Yukawa couplings to the SM fermions induce the decay into digluon and diphoton, i.e.  $H_3 \rightarrow gg, \gamma\gamma$ , analogous to the SM Higgs. Considering the flavor limits on the mixing angles  $\sin \theta_{1,2}$  below in Section 5, the fermion loops for both the  $\gamma\gamma$  and  $gg$  channels are highly suppressed. However, for the decay  $H_3 \rightarrow \gamma\gamma$ , there are extra contributions from the heavy  $W_R^\pm$ ,  $H_1^\pm$  and  $H_2^{\pm\pm}$  loops. In the low mass limit  $m_{H_3} \ll v_R$ , the diphoton channel is sensitive only to the RH scale  $\Gamma_{\gamma\gamma} \propto v_R^{-2}$  [27] and dominated by the  $W_R$  loop for TeV range  $v_R$ , as the scalar loops are comparatively suppressed by the loop function  $5A_0(0)/A_1(0) = -5/21$  [cf. Eq. (A.3)]. Similarly, the SM  $W$  loop is highly suppressed by the small  $W - W_R$  mixing  $\sin \zeta_W$  [cf. Eq. (3.16)]. The dominant two-body tree- and loop-level decay channels of  $H_3$  covering all the parameter space of interest for a light scalar  $m_{H_3} \lesssim m_h$  are presented in Appendix A, while the other decay channels, such as  $H_3 \rightarrow h^* h^* \rightarrow bbbb$ , are suppressed either kinematically or by the multi-particle phase space.

The decay branching ratios (BR) of  $H_3$  to the  $qq$ ,  $\ell^+ \ell^-$ ,  $\gamma\gamma$  and  $gg$  channels are presented in Figure 3 as functions of its mass and mixing with  $h$  (top panel) and  $H_1$  (bottom panel). For concreteness, we have made the following reasonable assumptions: (i) The RH scale  $v_R = 5$  TeV, which is close to the smallest value allowed by the current constraints on  $W_R$ . (ii) In the minimal LR model, the RH quark mixing matrix  $V_R$  is very similar to the CKM matrix  $V_L$ , up to some additional phases [28, 29]. For simplicity, we adopt  $V_R = V_L$  in the calculation. Thus with the experimental values of the SM quark masses and CKM mixing, we obtain the numerical values of the  $H_3$  couplings to the SM

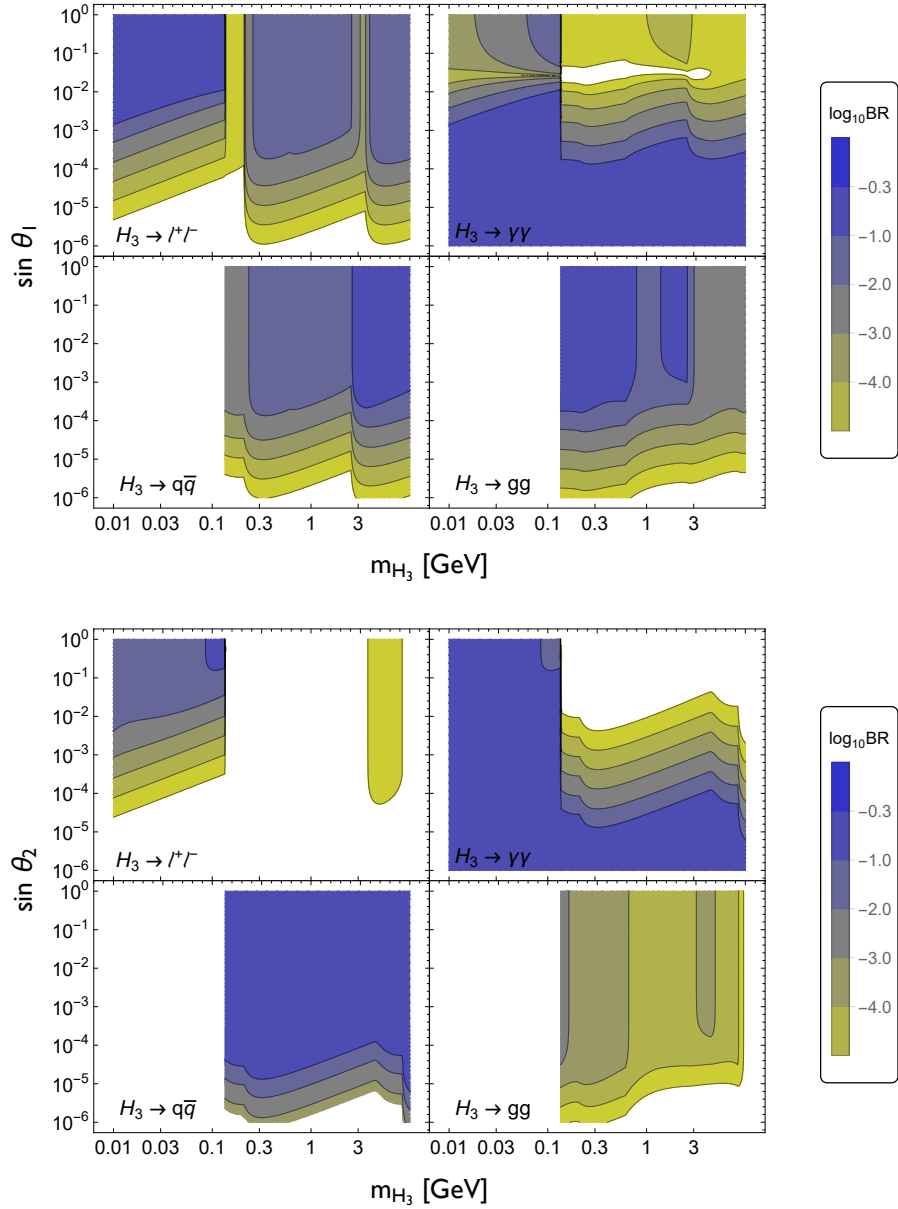


**Figure 3.** Color-coded branching ratios of  $H_3$  as functions of its mass and mixing with  $h$  (top) and  $H_1$  (bottom) for different decay modes. Here we have set the RH scale  $v_R = 5$  TeV and the RHN masses at 1 TeV.

quarks, including the FCNC couplings, arising from its mixing with the heavy scalar  $H_1$  [cf. Table 1]. (iii) The couplings of  $H_3$  to the charged leptons depend on the heavy and light neutrino masses and their mixings via the Yukawa coupling matrix  $Y_{\nu N}$ . Here we assume the three light neutrino masses are of normal hierarchy with the lightest one to be 0.01 eV, while all the three RHNs are assumed to be degenerate at 1 TeV without any RH lepton mixing, which pushes the couplings  $Y_{\nu N}$  to be very small, of order  $10^{-7}$  [cf. Eq. (3.18)]. Furthermore, when the  $H_3$  mass is below the pion mass, its decay to both

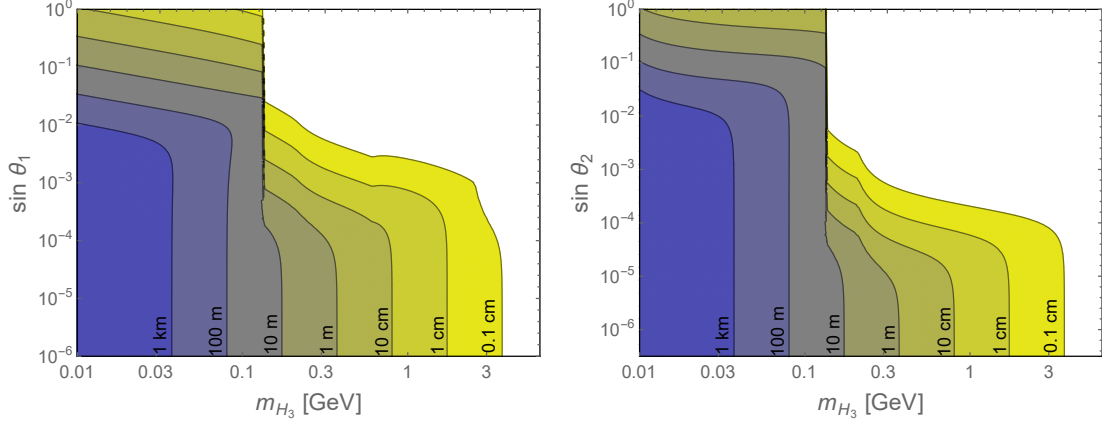


**Figure 4.** Contours of decay length of  $H_3$  at rest as a function of its mass and the mixing angles  $\sin \theta_{1,2}$ . Here we have set the RH scale  $v_R = 5$  TeV and the RHN masses at 1 TeV.

the quark and gluon channels are kinematically forbidden, as we do not have free hadronic states in Nature lighter than pions. For these hadronic channels, the RG running of the strong coupling constant  $\alpha_s$  is taken into consideration, which is important below the EW scale. The flavor violating decays of  $H_3$  in both the hadronic and leptonic sectors, e.g.  $H_3 \rightarrow sb, \mu\tau$ , are included in making the plots in Figure 3.

From Figure 3, we find that when the mixing angles are sizable,  $H_3$  decays mostly into the SM quarks (above the pion mass threshold) and charged leptons (below the pion mass), while when  $\sin \theta_{1,2} \lesssim 10^{-4}$ , the dominant decay of  $H_3$  is into the diphoton channel, which benefits from the heavy gauge boson loops induced by the RH gauge coupling (independent of  $\sin \theta_{1,2}$ ), with a sub-dominant contribution from the heavy scalar loops. With large BR to two photons, the FCNC constraints can be used to set limits on the mixing angles  $\sin \theta_{1,2}$  as a function of  $m_{H_3}$ ; see more details in Section 5.

Using the partial decay widths given in Appendix A, we calculate the total decay length  $L_0$  of  $H_3$  at rest, as shown in Figure 4, as a function of its mass and mixing with  $h$  (left panel) and  $H_1$  (right panel). From these lifetime contours, it is obvious that when the scalar  $H_3$  mass is in the GeV range, its *proper* decay length  $L_0 \sim \mathcal{O}(1)$  cm. When  $H_3$  is produced at the LHC, it will be boosted by a Lorentz factor of  $E_{H_3}/m_{H_3} \sim \mathcal{O}(100)$ , so the decay length  $L$  in the laboratory frame would reach the scale of meters, thus making it a natural LLP candidate and leading to spectacular displaced vertex signals. For even smaller masses,  $m_{H_3} \sim \mathcal{O}(100)$  MeV, the decay length is much longer, of order 100 m. More details of displaced vertex and LLP searches are presented in Section 6.

## 4 Cosmological constraints

Light particles can have an impact on the cosmological history of our Universe, depending on their decay properties. In our model, the  $H_3$  particle is produced in the early Universe by various processes mediated by heavy scalars and gauge bosons, but at temperatures  $T \ll m_{Z'}, m_{W_R}, m_h$ , the dominant process that keeps  $H_3$  in equilibrium is  $\gamma\gamma \rightarrow H_3$ .

For a GeV-scale  $H_3$ , it stays in equilibrium till below its mass and decouples at a lower temperature  $T_*$ , which can be estimated by equating the rate of the process  $\gamma\gamma \leftrightarrow H_3$  to the Hubble expansion rate:

$$\frac{\alpha^2 T_*^3 x^{3/2} e^{-x}}{1048\pi^3} \leq \frac{10T_*^2}{M_{\text{Pl}}}, \quad (4.1)$$

where  $x = m_{H_3}/T_*$ ,  $\alpha \equiv e^2/4\pi$  is the fine structure constant and  $M_{\text{Pl}}$  is the Planck mass. Another relevant parameter is the decay temperature which is determined by the condition  $T_d = \sqrt{\Gamma_{H_3} H(T_d)}$ , where  $\Gamma_{H_3}$  is the total decay rate of  $H_3$  (thermal averaged) and  $H(T_d)$  is the Hubble expansion rate at temperature  $T_d$ . Typically, one requires either (i)  $T_d \geq \Lambda_{\text{QCD}} \sim 150$  MeV, the QCD phase transition temperature, so that the primordial synthesis of light elements and the ratio of their abundances is not affected much from their SM predicted values; or (ii)  $T_* \geq T_{\text{BBN}} \sim 1$  MeV, so that the light particle does not contribute like an extra degree of freedom at the epoch of Big Bang Nucleosynthesis (BBN). In our model,  $T_d \gg T_*$  till the BBN epoch, and therefore, the condition (ii) is more stringent. Thus, we find that as long as  $T_* \geq 1$  MeV (or the epoch of BBN), the  $H_3$  particle will decouple and then decay to photons which will then thermalize with the rest of the cosmic soup (e.g. by Compton scattering) and it will not affect the nucleosynthesis discussion. On the other hand, if  $T_*$  is below the epoch of BBN, the  $H_3$  particle is in equilibrium with the thermal soup and will contribute like an extra boson species and being spin zero will contribute  $4/7$  to  $\Delta N_{\text{eff}}$ , which is incompatible with the Planck bounds at the  $2.5\sigma$  level [30]. Using Eq. (4.1) and setting  $T_* \geq 1$  MeV, we therefore obtain a conservative lower bound on  $m_{H_3} \gtrsim 20$  MeV, which will be applied to our subsequent discussion. A more accurate cosmological lower bound on  $m_{H_3}$  might be obtained by solving the relevant Boltzmann equations and calculating the temperature rise of the thermal plasma due to energy injection from the  $H_3$  decay, but such a detailed analysis is beyond the scope of this work and will be given elsewhere.

## 5 Laboratory Constraints

The light scalar  $H_3$  mixing with the heavy flavor-changing scalar  $H_1$  induces flavor-changing couplings of  $H_3$  to the SM quarks and charged leptons [cf. Table 1], which are severely constrained by the low-energy flavor data, e.g. the  $K^0 - \bar{K}^0$ ,  $B_d - \bar{B}_d$  and  $B_s - \bar{B}_s$  meson oscillations and rare  $K$  and  $B$  meson decays.<sup>1</sup> In addition, the  $H_3$  couplings are also limited by the SM invisible decay, rare top and  $Z$  boson decay, which are either absent or highly suppressed in the SM. In this section, we collect all these laboratory constraints on the  $h - H_3$  and  $H_1 - H_3$  mixing angles  $\theta_{1,2}$ , as well as their future prospects, which will provide useful guidelines for the collider searches for  $H_3$  in the dominant  $\gamma\gamma$  channel, as we will discuss in Section 6.

### 5.1 $K$ and $B$ meson oscillations

It should be emphasized that although the flavor-changing couplings of  $H_3$  originate from the heavy scalar  $H_1$ , the masses of  $H_1$  and  $H_3$  are independent observables (proportional

---

<sup>1</sup>The constraints from  $D$  meson sector are much weaker and thus not considered here.

respectively to  $\sqrt{\alpha_3}$  and  $\sqrt{\rho_1}$  at the leading order), therefore the constraints on  $H_3$  derived here from flavor oscillations are different from those on the heavy scalar  $H_1$  derived earlier in Ref. [17, 31]. Furthermore, the constraints on the mixing angles  $\sin \theta_{1,2}$  from meson oscillations is sensitive to the mass of  $H_3$ , especially when  $m_{H_3}$  is comparable to the  $K$  or  $B$  meson masses.

Taking the  $K^0 - \bar{K}^0$  mixing as an explicit example, the effective four-fermion interactions mediated by  $H_3$  can be cast into linear combinations of the effective dimension-6 operators of form [32]

$$\mathcal{O}_2 = [\bar{s}(1 - \gamma_5)d][\bar{s}(1 - \gamma_5)d], \quad (5.1)$$

$$\tilde{\mathcal{O}}_2 = [\bar{s}(1 + \gamma_5)d][\bar{s}(1 + \gamma_5)d], \quad (5.2)$$

$$\mathcal{O}_4 = [\bar{s}(1 - \gamma_5)d][\bar{s}(1 + \gamma_5)d]. \quad (5.3)$$

Though the flavor-changing couplings of  $H_3$  to the SM fermions are from the mixing with  $h$  and  $H_1^0$  (cf. the  $\sin \tilde{\theta}_2$  terms of the Yukawa couplings in Table 1), but here they are not simply multiplied by a factor of  $\sin \tilde{\theta}_2$ . This is because the operators of form  $\mathcal{O}_2$  and  $\tilde{\mathcal{O}}_2$  are absent in the  $H_1$  case, which are canceled by the CP-odd scalar  $A_1$  in the mass degenerate limit of  $m_{H_1^0} = M_{A_1^0}$ . In short, the effective Lagrangian we need is

$$\begin{aligned} \mathcal{L}_{H_3} = \frac{G_F}{4\sqrt{2}} \frac{\sin^2 \tilde{\theta}_2}{m_K^2 - m_{H_3}^2 + im_{H_3}\Gamma_{H_3}} & \left[ \left( \sum_i m_i \lambda_i^{RL} \right)^2 \mathcal{O}_2 + \left( \sum_i m_i \lambda_i^{LR} \right)^2 \tilde{\mathcal{O}}_2 \right. \\ & \left. + 2 \left( \sum_i m_i \lambda_i^{LR} \right) \left( \sum_i m_i \lambda_i^{RL} \right) \mathcal{O}_4 \right], \quad (5.4) \end{aligned}$$

where  $G_F$  is the Fermi constant,  $m_i = \{m_u, m_c, m_t\}$  the running up-type quark masses,  $\lambda_i^{LR} = V_{L,i2}^* V_{R,i1}$  and  $\lambda_i^{RL} = V_{R,i2}^* V_{L,i1}$  the left- and right-handed quark mixing matrix elements. For simplicity we have assumed that  $V_R = V_L$  which is a good approximation in the minimal LR model, up to some additional CP violating phases in the RH matrix [28, 29]. As for the heavy scalars  $H_1$  and  $A_1$ , the charm quark dominates the mass and quark mixing terms, i.e.  $m_c \lambda$  ( $\lambda$  being the Cabibbo angle), with sub-leading term from the top quark  $\sim m_t \lambda^5$ .

To calculate the contribution of Lagrangian (5.4) to the  $K^0 - \bar{K}^0$  mixing, we need to know the hadronic matrix elements when the operators are sandwiched by the  $K^0$  states:

$$\langle K^0 | \mathcal{O}_i | \bar{K}^0 \rangle = N_i m_K f_K^2 B_i(\mu) R_K^2(\mu), \quad (5.5)$$

with  $i = 2, 4$ , and the  $K$  decay constant  $f_K = 113$  MeV,  $N_2 = 5/3$ ,  $N_4 = -2$  and the parameters  $B_2 = 0.679$ ,  $B_4 = 0.810$  from lattice calculation [32]. The mass ratio factor  $R_K = m_K/(m_d + m_s)$  is evaluated at the energy scale  $\mu = 2$  GeV. As the strong interaction conserves parity, we have  $\langle K^0 | \tilde{\mathcal{O}}_2 | \bar{K}^0 \rangle = \langle K^0 | \mathcal{O}_2 | \bar{K}^0 \rangle$ . Then the  $K^0$  mass difference

$$\Delta m_K \simeq 2 \text{Re} \sum_i \eta_i(\mu) \langle K^0 | \mathcal{L}_{H_3}^{(i)} | \bar{K}^0 \rangle \quad (5.6)$$

with  $\eta_2 = 2.052$  and  $\eta_4 = 3.2$  the QCD radiative corrections running from the EW scale down to the scale of  $\mu \sim 2$  GeV [33].

On the experimental side, the  $K^0 - \bar{K}^0$  mixing has been measured to a high accuracy, i.e.  $\Delta m_K = (3.473 \pm 0.006) \times 10^{-15}$  GeV [34]; on the theoretical side, the short- and long-distance contributions to  $\Delta m_K$  are much larger than the experimental errors, up to 20% of the central value. Conservatively we use 50% of the experimental central value [17] to set upper limits on the mixing angles  $\sin \theta_{1,2}$ , as shown in Figure 5 (blue solid lines). As expected, in the (narrow) resonance region where  $m_{H_3} \simeq m_K$  the limit on the mixing angles could be largely strengthened. When the  $H_3$  mass gets lower, the  $H_3$  propagator is dominated by the momentum term

$$\frac{1}{q^2 - m_{H_3}^2 + im_{H_3}\Gamma_{H_3}} \rightarrow \frac{1}{q^2} \simeq \frac{1}{m_K^2}, \quad (5.7)$$

and the limits approach to a constant value. On the other hand, when  $m_{H_3} \gg m_K$ , the constraints are similar to that for the heavy scalar  $H_1$ , and scale as  $\sin \theta_{1,2}^{\text{limit}} \propto m_{H_3}$ .

The calculation of flavor constraints from  $B_d - \bar{B}_d$  and  $B_s - \bar{B}_s$  mixings are quite similar to those from  $K^0$ , with the QCD correction coefficient  $\eta_2 = 1.654$  and  $\eta_4 = 2.254$  at the  $B$  meson scale [33], and the  $B$ -parameters for the effective operators with respect to the bottom quark and  $d$  quark (or the  $s$  quark) are respectively [35]

$$\begin{aligned} B_2(B_d) &= 0.82, & B_4(B_d) &= 1.16, \\ B_2(B_s) &= 0.83, & B_4(B_s) &= 1.17. \end{aligned} \quad (5.8)$$

Different from the  $K$  meson case, for the  $B_{d,s}$  mesons, the top quark contribution dominates in Eq. (5.4), which largely improves the effective coupling  $\sum_i m_i \lambda_i^{LR, RL}$  and strengthens the limits on the coupling of  $H_3$  to the bottom quark. The experimental values of  $\Delta m_{B_{d,s}}$  agree well with the SM predictions [34], allowing new physics contributions of only  $9.3 \times 10^{-14}$  GeV and  $2.7 \times 10^{-12}$  GeV respectively at the  $2\sigma$  level by the current CKM fitter global fit, when CP violation is neglected [36]. The corresponding upper limits on the mixing angles  $\sin \theta_{1,2}$  are presented in Figure 6. The  $B$  mesons are roughly 10 times heavier than the  $K$  meson, and the absolute values of error bars for the  $B$  mass differences are much larger than  $\Delta m_K$ , thus the limits for the case of  $m_{H_3} \lesssim m_{\text{meson}}$  is weaker for the  $B$  mixing case than that from  $K$  mixing. However, this could be partially compensated by the large effective coupling  $\sum_i m_i \lambda_i^{LR, RL}$  when  $H_3$  is heavier, especially for the  $B_d$  meson. Thus when  $m_{H_3} \gtrsim m_b$ , the limits on  $\sin \tilde{\theta}_2$  from the  $B$  meson mixings turn out to be more stringent.

## 5.2 Meson decay

Since  $H_3$  acquires flavor-changing couplings to the SM quarks via its mixing with the heavy Higgs  $H_1$ , it could be produced from the flavor changing decay of  $K$  and  $B$  mesons, when kinematically allowed. The constraints coming from the up-sector FCNC are very weak and we do not discuss them here. In the down-type quark sector, we have the parton-level processes  $b \rightarrow dH_3$ ,  $sH_3$  and  $s \rightarrow dH_3$  at the tree level. Depending on the mass  $m_{H_3}$

and the mixing angles  $\sin\theta_{1,2}$ , after being produced in  $K$  or  $B$  decays,  $H_3$  will decay into dileptons  $\ell^+\ell^-$ , hadronic states  $q\bar{q}$ ,  $gg$ , or two photons  $\gamma\gamma$ , with the invariant mass of the final states close to the  $H_3$  mass. Thus, we should expect flavor-violating signals of the form

$$d_j \rightarrow d_i H_3^0, \quad \text{with } H_3 \rightarrow \text{leptons, hadrons, photons.} \quad (5.9)$$

The corresponding SM decay modes, like  $B^+ \rightarrow K^+ \gamma\gamma$ , are generally highly suppressed by the CKM matrix elements and loop factors, thus these rare decay channels are expected to set severe limits on the mixing angles  $\sin\theta_{1,2}$  and hence the flavor changing couplings of  $H_3$  to quarks.

The most stringent bounds on the decay branching ratios for the process (5.9) from various low-energy flavor experiments are collected in Table 2, some of which follow to some extent the discussion of Refs. [37–40]. The first simple but robust limits come from the observed total widths of  $K$  and  $B$  mesons, which depend only on the flavor-changing couplings of  $H_3$  but not on how  $H_3$  decays or the details of FCNC data. The lifetimes of  $K^\pm$  and  $K^0$  are both precisely measured to the level of  $10^{-3}$ , however the absolute theoretical values are subject to a large uncertainty of the strange quark mass, up to the order of 10% [34]. Thus, to be conservative, we take 20% of the experimental values to constrain the light scalar  $H_3$ , which are respectively  $1.33 \times 10^{-17}$  GeV and  $3.21 \times 10^{-18}$  GeV when converted to the maximum allowed discrepancy in the total widths of  $K^\pm$  and  $K^0$ . On the other hand, for the  $B$  meson, though the lifetime ratios such as  $\tau_{B^\pm}/\tau_{B^0}$  can be determined up to the level of a few %, the absolute values of  $\tau_B$  are subject to large uncertainties in the form factors, at the level of 10% [34]. The  $2\sigma$  lifetime uncertainties lead to an allowed discrepancy of up to  $1.05 \times 10^{-13}$  GeV in the total decay width of  $B$  mesons. The  $K$  and  $B$  meson width limits on  $\sin\theta_{1,2}$  are shown in Figures 5 and 6 as functions of  $m_{H_3}$ . All the regions above these lines are excluded, wherein the flavor-changing decays are enhanced by the large mixing angles.

Before going into the details of other meson decay limits, let us make some general comments on the constraints from meson decays. Roughly speaking, regarding the flavor changing couplings mediated by  $H_3$ , there are essentially two different classes of experiments that are applicable to our case. The first ones are the *visible* decays, i.e. those with visible SM particles in the final state such as  $K^+ \rightarrow \pi^+ \gamma\gamma$  and  $B \rightarrow K \mu^+ \mu^-$ . The SM backgrounds for these rare decays are generally very small, and the tree-level flavor-changing couplings of  $H_3$  could be severely constrained. However, the sensitivity depends largely on the selection procedure of signals, e.g. the vetoes, cuts and detector position and energy resolutions etc. The second class of processes are the *invisible* decays, i.e. the signal of type  $d_j \rightarrow d_i + \text{inv.}$  at the parton level. The invisible part, or missing energy at colliders, could be from the neutrinos, such as  $K^+ \rightarrow \pi^+ \nu \bar{\nu}$ . We include in this category the null result of dedicated searches for a light neutral particle  $X^0$  from meson decay, e.g.  $K^+ \rightarrow \pi^+ X^0$ , with the light particle long-lived enough to escape from the detector without leaving any observable footprints. These invisible decays are expected to be very sensitive to the scalar  $H_3$  which is an LLP from the detector perspective, as long as it is light and the mixings  $\sin\theta_{1,2}$  are small. In this case, we take the conservative assumption that the

**Table 2.** Summary of meson decay constraints used to derive current/future limits on the mixing angles in Figures 5, 6 and 7. The last column gives the upper limit on the BR of the process used in our calculation. The corresponding numbers (in parenthesis) for the beam-dump experiments (last six rows) give the limit on the number of events.

Experiment	Meson decay	$H_3$ decay	$E_{H_3}$	Decay length	Limit on BR ( $N_{\text{event}}$ )
NA48/2 [43]	$K^+ \rightarrow \pi^+ H_3$	$H_3 \rightarrow e^+ e^-$	$\sim 30$ GeV	$< 0.1$ mm	$2.63 \times 10^{-7}$
NA48/2 [44]	$K^+ \rightarrow \pi^+ H_3$	$H_3 \rightarrow \mu^+ \mu^-$	$\sim 30$ GeV	$< 0.1$ mm	$8.88 \times 10^{-8}$
NA62 [46]	$K^+ \rightarrow \pi^+ H_3$	$H_3 \rightarrow \gamma\gamma$	$\sim 37$ GeV	$< 0.1$ mm	$4.70 \times 10^{-7}$
E949 [47–50]	$K^+ \rightarrow \pi^+ H_3$	any (inv.)	$\sim 355$ MeV	$> 4$ m	$4 \times 10^{-10}$
NA62 [52]	$K^+ \rightarrow \pi^+ H_3$	any (inv.)	$\sim 37.5$ GeV	$> 2$ m	$2.4 \times 10^{-11}$
KTeV [54]	$K_L \rightarrow \pi^0 H_3$	$H_3 \rightarrow e^+ e^-$	$\sim 30$ GeV	$< 0.1$ mm	$2.8 \times 10^{-10}$
KTeV [55]	$K_L \rightarrow \pi^0 H_3$	$H_3 \rightarrow \mu^+ \mu^-$	$\sim 30$ GeV	$< 0.1$ mm	$4 \times 10^{-10}$
KTeV [56, 57]	$K_L \rightarrow \pi^0 H_3$	$H_3 \rightarrow \gamma\gamma$	$\sim 40$ GeV	$< 0.1$ mm	$3.71 \times 10^{-7}$
BaBar [60]	$B \rightarrow K H_3$	$H_3 \rightarrow \ell^+ \ell^-$	$\sim m_B/2$	$< 0.1$ mm	$7.91 \times 10^{-7}$
Belle [61]	$B \rightarrow K H_3$	$H_3 \rightarrow \ell^+ \ell^-$	$\sim m_B/2$	$< 0.1$ mm	$4.87 \times 10^{-7}$
LHCb [62]	$B^+ \rightarrow K^+ H_3$	$H_3 \rightarrow \mu^+ \mu^-$	$\sim 150$ GeV	$< 0.1$ mm	$4.61 \times 10^{-7}$
BaBar [67]	$B \rightarrow K H_3$	any (inv.)	$\sim m_B/2$	$> 3.5$ m	$3.2 \times 10^{-5}$
Belle II [64]	$B \rightarrow K H_3$	any (inv.)	$\sim m_B/2$	$> 3$ m	$4.1 \times 10^{-6}$
LHCb [70]	$B_s \rightarrow \mu\mu$	—	—	—	$2.51 \times 10^{-9}$
BaBar [76]	$B_d \rightarrow \gamma\gamma$	—	—	—	$3.3 \times 10^{-7}$
Belle [77]	$B_s \rightarrow \gamma\gamma$	—	—	—	$3.1 \times 10^{-6}$
BaBar [80]	$\Upsilon \rightarrow \gamma H_3$	$H_3 \rightarrow qq, gg$	$\sim m_\Upsilon/2$	$< 3.5$ m	$[1, 80] \times 10^{-6}$
CHARM [83]	$K \rightarrow \pi H_3$	$H_3 \rightarrow \gamma\gamma$	$\sim 10$ GeV	[480, 515] m	$(< 2.3)$
CHARM [83]	$B \rightarrow X_s H_3$	$H_3 \rightarrow \gamma\gamma$	$\sim 10$ GeV	[480, 515] m	$(< 2.3)$
SHiP [84]	$K \rightarrow \pi H_3$	$H_3 \rightarrow \gamma\gamma$	$\sim 25$ GeV	[70, 125] m	$(< 3)$
SHiP [84]	$B \rightarrow X_s H_3$	$H_3 \rightarrow \gamma\gamma$	$\sim 25$ GeV	[70, 125] m	$(< 3)$
DUNE [85]	$K \rightarrow \pi H_3$	$H_3 \rightarrow \gamma\gamma$	$\sim 12$ GeV	[500, 507] m	$(< 3)$
DUNE [85]	$B \rightarrow X_s H_3$	$H_3 \rightarrow \gamma\gamma$	$\sim 12$ GeV	[500, 507] m	$(< 3)$

sensitivity depends only on the detector size but not too much on the data analysis. For these two distinct categories of searches, we use the following two branching ratios to set limits on the mixing angles  $\sin \theta_{1,2}$  and  $m_{H_3}$ :

$$\text{visible : } \text{BR}(d_j \rightarrow d_i H_3) \text{BR}(H_3 \rightarrow \chi\chi) \left[ \exp\left(-\frac{L\Gamma_{H_3}}{b}\right) - \exp\left(-\frac{(L + \Delta L)\Gamma_{H_3}}{b}\right) \right], \quad (5.10)$$

$$\text{invisible : } \text{BR}(d_j \rightarrow d_i H_3) \exp\left(-\frac{R\Gamma_{H_3}}{b}\right), \quad (5.11)$$

where  $\chi\chi = \ell^+ \ell^-$ , hadrons and  $\gamma\gamma$  are the visible SM particles,  $b$  is the Lorentz boost factor,  $L$  and  $\Delta L$  denote respectively the distance from the primary production vertex and the decay length when  $H_3$  decays into visible particles in the detector, and  $R$  denotes the detector size in the invisible final state case. The two different search strategies are largely complementary to each other, when applied to constrain the light scalar  $H_3$  in the LR model.

### 5.2.1 $K$ meson decay

The partial width for the charged  $K$  meson decay is given by [39, 40]

$$\Gamma(K^\pm \rightarrow \pi^\pm H_3) = \frac{G_F m_{K^\pm} \sin^2 \tilde{\theta}_2}{8\sqrt{2}\pi} \left| \sum_i m_i \lambda_{i,21}^{RL} \right|^2 \left( 1 - \frac{m_{\pi^\pm}^2}{m_{K^\pm}^2} \right)^2, \quad (5.12)$$

where the kinetic function  $\beta_2$  is defined in Eq. (A.5). For a CP-even scalar, the decay width for the neutral  $K$  meson, i.e.  $K_L \rightarrow \pi^0 H_3$  is related to the charged counterpart by taking the real part of the amplitude in Eq. (5.12) [41].

The  $\text{BR}(K^+ \rightarrow \pi^+ e^+ e^-)$  and  $\text{BR}(K^+ \rightarrow \pi^+ \mu^+ \mu^-)$  are predicted to be respectively  $(3.9 \pm 0.8) \times 10^{-7}$  and  $(1.2 \pm 0.3) \times 10^{-7}$  in the SM [42]. Taking the largest discrepancy of the theoretical and experimental values from NA48/2 [43, 44] at the  $2\sigma$  C.L., we obtain the maximum allowed contribution from potential beyond SM physics, which are listed in the last column of Table 2. Regarding the rare kaon decay with two photons in the final state, i.e.  $K^+ \rightarrow \pi^+ \gamma \gamma$ , we adopt the SM prediction of  $(9.66 \pm 3.43) \times 10^{-7}$  with the invariant mass of diphoton  $(m_{\gamma\gamma}/m_K)^2 > 0.2$  [45]. Comparing it to the measurement at NA62 [46], we arrive at the BR limit of  $4.70 \times 10^{-7}$  at  $2\sigma$  C.L.

The kaon beam energy at NA48/2 is around  $E_{\text{NA}} \simeq 60$  GeV or slightly higher, which leads to a large boost factor of  $b \simeq E_{\text{NA}}/2m_{H_3}$  in Eq. (5.10). The position resolution of the detector could reach up to  $\lesssim 1$  mm; if the LLP  $H_3$  were produced in these experiments, the signal would be very different from the SM processes: i.e. there would be displaced  $ee$ ,  $\mu\mu$  or  $\gamma\gamma$  tracks from the primary kaon vertex, which could be easily identified in the detector layers. To be concrete, we adopt a smaller decay length of  $\Delta L = 0.1$  mm, which is more conservative than in Refs. [38, 40]. Compared to the invisible decays with  $H_3$  leaving no trace in the detector, the visible searches are more sensitive to shorter-lived  $H_3$  with larger mixing angles  $\sin \theta_{1,2}$ . The excluded regions from  $K^+ \rightarrow \pi^+ \ell \ell$  are presented in the plots of Figure 5.

In the invisible searches, the most stringent bounds are from the process  $K^+ \rightarrow \pi^+ \nu \bar{\nu}$  in the experiment E949 [47–50], with neutrinos in the final state. In calculation of the limits using Eq. (5.11), we set  $E_K \simeq 710$  MeV [51], adopt conservatively the decay length  $L = 4$  m [39]<sup>2</sup>, and use the BR limits of  $4 \times 10^{-10}$  [47–49] to set separate limits on  $\sin \theta_1$  and  $\sin \theta_2$  by setting the other to be zero, as functions of  $H_3$  mass, as shown in Figure 5. When  $m_{H_3}$  is close to  $m_\pi$ , we adopt the limit from  $K^+ \rightarrow \pi^+ \pi^0$  with  $\pi^0 \rightarrow \nu \bar{\nu}$  [50], which is less constraining, with the BR up to  $6 \times 10^{-8}$ .

The limits from  $K^+ \rightarrow \pi^+ \nu \bar{\nu}$  is expected to be more stringent at the proposed running of NA62 [52], with a precision up to 10% of the SM value [52]. The theoretical uncertainty is below 4% [53], thus we take the expected largest  $2\sigma$  total uncertainties  $2 \times (0.10 + 0.04) \times 8.4 \times 10^{-11} = 2.35 \times 10^{-11}$  as the expected NA62 limit to constrain the couplings of  $H_3$ , assuming the measurement of NA62 agrees well with the SM prediction.

The rare decays of neutral kaon  $K_L \rightarrow \pi^0 \chi \chi$  have been searched for at the KTeV experiment, with lepton pairs  $\chi \chi = e^+ e^-$ ,  $\mu^+ \mu^-$  [54, 55] or diphoton  $\gamma \gamma$  [56] in the final state. The BRs are constrained to be very small, especially for the dileptons. Similar to

<sup>2</sup>A smaller decay length will make the constraints more stringent, see Ref. [38].

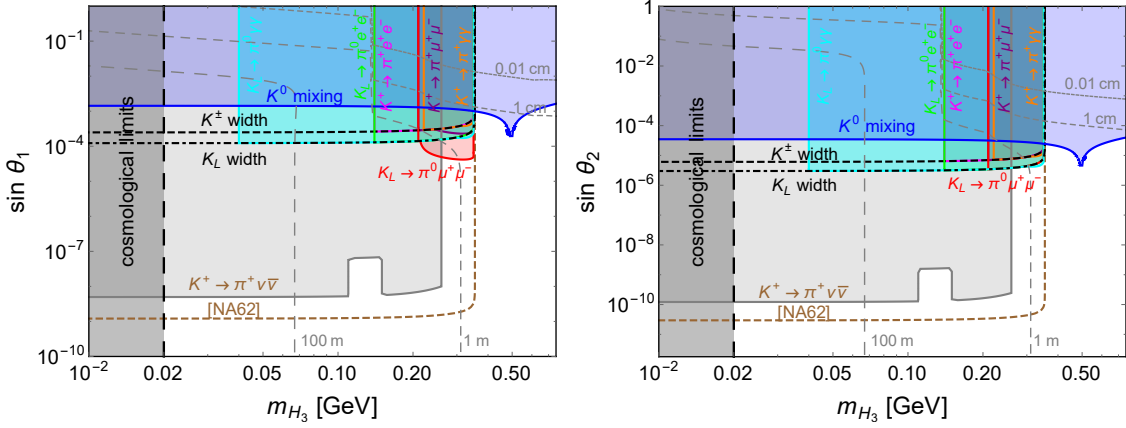


**Figure 5.** Flavor changing limits on the mixing angles  $\sin \theta_{1,2}$  and  $m_{H_3}$  from  $K - \bar{K}$  mixing (blue) and various charged and neutral kaon decay modes:  $K^\pm \rightarrow \pi^\pm \chi\chi$ , in the final state of leptons  $\chi\chi = e^+e^-$  [43],  $\mu^+\mu^-$  [44] or  $\gamma\gamma$  [46] in the NA48/2 and NA62 experiments, and  $K_L \rightarrow \pi^0 \chi\chi$ , in the final state of leptons  $\chi\chi = e^+e^-$  [54],  $\mu^+\mu^-$  [55] or  $\gamma\gamma$  [56, 57] in the KTeV experiment. The invisible limits from  $K^\pm \rightarrow \pi^\pm \nu\bar{\nu}$  is from the E949 experiment [47–50]. The dashed brown curve is the expected sensitivity from NA62 [52]. The dashed (dot-dashed) black curve is the limit from the total  $K^\pm$  ( $K_L$ ) width, whereas  $m_{H_3} \lesssim 20$  MeV (vertical black-shaded) is disfavored from BBN considerations (cf. Section 4). The dashed gray lines are the *proper* lifetime of  $H_3$  with values of 0.01 cm, 1 cm, 1 m, and 100 m. See text for more details.

the visible  $K^\pm$  decay at NA48/2 and NA62, the kaon system is highly boosted, with a total energy ranging from 20 GeV to 220 GeV for the dilepton searches, and 40 GeV to 160 GeV for the diphoton decay. Examining the energy distribution, we take the mean energy to be 30 and 40 GeV for the kaon system. Assuming a decay length of  $\Delta L = 1$  mm, we get the visible decay limits as shown in Figure 5. Around the  $\pi^0$  mass, due to the resonance effect, the SM production rate of  $K_L \rightarrow \pi^0 \pi^0$  is much larger than elsewhere, and we use the SM  $\text{BR}(K_L \rightarrow \pi^0 \pi^0) = 9 \times 10^{-4}$  to set limits on  $H_3$  [57].

### 5.2.2 B meson decay

The partial width for the exclusive  $B$  meson decay is very similar to that for  $K$  meson [cf. Eq. (5.12)]:

$$\Gamma(B \rightarrow KH_3) = \frac{G_F m_B \sin^2 \tilde{\theta}_2}{8\sqrt{2}\pi} \left| \sum_i m_i \lambda_{i,32}^{RL} \right|^2 \left( 1 - \frac{m_K^2}{m_B^2} \right)^2 \left[ f_0^{(K)}(m_{H_3}^2) \right]^2 \times \beta_2(m_B, m_K, m_{H_3}), \quad (5.13)$$

where  $f_0(q^2)$  is a form factor of the form [58]

$$f_0(q^2) = \frac{r^2}{1 - q^2/m_{\text{fit}}^2}, \quad (5.14)$$

where for the  $K$  meson final state, the parameters are  $r_2 = 0.330$  and  $m_{\text{fit}}^2 = 37.46 \text{ GeV}^2$ . For the inclusive  $B$  decays, we have

$$\Gamma(B \rightarrow X_s H_3) = \frac{G_F m_B \sin^2 \tilde{\theta}_2}{4\sqrt{2}\pi} \left| \sum_i m_i \lambda_{i,32}^{RL} \right|^2 \left( 1 - \frac{m_{H_3}^2}{m_B^2} \right)^2, \quad (5.15)$$

with  $X_s$  standing for any strange-flavored meson.

In the SM, the BR of flavor changing decay  $B \rightarrow K\ell^+\ell^-$  ( $\ell = e, \mu$ ) is predicted to be  $5.7 \times 10^{-7}$ , with large uncertainties from the form factor, top quark mass etc, summing up to 35% [59]. Comparing the theoretical prediction to the measurements at BaBar  $((6.5 \pm 1.5) \times 10^{-7})$  [60], Belle  $((4.8 \pm 0.58) \times 10^{-7})$  [61], and LHCb  $((4.36 \pm 0.23) \times 10^{-7})$  [62] and taking the largest  $2\sigma$  discrepancies of theoretical and experimental values, we collect the BR limits in Table 2. The three detectors all have very good spatial resolutions [63–65]; to be concrete we take  $\Delta L \sim 0.1 \text{ mm}$ , and setting  $L = 0$  in Eq. (5.10) for all of them, we obtain the excluded regions shown in in Figure 6. Again, for the  $B$  mesons at LHCb, the average energy of the  $B$  meson is  $E_B^{(\text{LHCb})} \sim 300 \text{ GeV}$ , so we have a large boost factor. Compared to the  $K$  decays, the flavor changing coupling to  $b$  quark is largely enhanced by the factor  $\sum_i m_i \lambda_{i,32}^{RL}$ . When  $m_{H_3} \sim m_{J/\psi}$  or  $m_{\psi(2S)}$ , we use the SM BRs to set limits on  $H_3$  [34, 39]:

$$\text{BR}(B \rightarrow K J/\psi) = \text{BR}(B \rightarrow K\ell^+\ell^-) = 5 \times 10^{-5}, \quad (5.16)$$

$$\text{BR}(B \rightarrow K\psi(2S)) = \text{BR}(B \rightarrow K\ell^+\ell^-) = 5 \times 10^{-6}. \quad (5.17)$$

With more  $B$  mesons collected at Belle II [64], the constraints in the visible modes could be further strengthened.

A light neutral scalar has been searched for in the decay  $B \rightarrow KX^0$  in the CLEO experiment [66], with an upper limit at the level of  $5.3 \times 10^{-5}$ . The rare decays of  $B \rightarrow K\nu\bar{\nu}$  at BaBar leads to a more stringent limit: combining both the channels of  $B^+ \rightarrow K^+\nu\bar{\nu}$  and  $B^0 \rightarrow K^0\nu\bar{\nu}$ , the BR is less than  $3.2 \times 10^{-5}$  at the 90% C.L. [67],<sup>3</sup> with the SM prediction of  $\text{BR}(B \rightarrow K\nu\bar{\nu}) = (4.5 \pm 0.7) \times 10^{-6}$  [68]. With a detector size of  $L = 3.5 \text{ m}$  [63], we can exclude large region in the plane of  $m_{H_3} - \sin\theta_{1,2}$ , as shown in Figure 6. As for the visible  $B$  decays, though the absolute value of the limit on  $\text{BR}(B \rightarrow K\nu\bar{\nu})$  is much smaller than that from  $\text{BR}(K \rightarrow \pi\nu\bar{\nu})$ , the  $B$  meson decay is comparatively enhanced by the larger flavor changing coupling of  $\sum_i m_i \lambda_{i,32}$ , with respect to the coupling of  $\sum_i m_i \lambda_{i,21}$  for the  $K$  mesons. With a total luminosity of  $50 \text{ ab}^{-1}$  at SuperKEKB, the  $B^+ \rightarrow K^+\nu\bar{\nu}$  could be measured up to 30% of the SM BR at Belle II [64], i.e.  $1.5 \times 10^{-6}$ . Applied to the LR model, this means the flavor changing couplings to  $b$  quark could be more severely constrained, as demonstrated by the dashed blue lines in Figure 6.

With the flavor-changing couplings to the quarks in  $B$  mesons,  $H_3$  could also be produced off-shell from  $B$  meson decay and then decays into light SM particles, such as the

---

<sup>3</sup>There are also searches of  $B \rightarrow K^*\nu\bar{\nu}$  [64, 67], but the limits are comparatively less constraining, thus we consider here only the  $K$  mesons in the final state.



the box diagrams with  $H_3$  propagators for the couplings  $bq\gamma\gamma$ , the triangular diagrams for the trilinear coupling  $bq\gamma$  and the  $H_3$  mediated  $bq$  bilinear coupling; the second class are those with an  $s$ -channel  $H_3$  coupled to the two photons via the fermion, scalar and gauge boson loops. It is expected that the second class of diagrams dominates, producing the partial width [74, 75]

$$\Gamma(B_q \rightarrow \gamma\gamma) = \frac{\alpha^3 m_{B_q}^5 f_{B_q}^2}{128\pi^2 s_W^2 m_W^2} \frac{|\mathcal{Y}_{d,qb}|^2}{|m_{B_q}^2 - m_{H_3}^2 + im_{H_3}\Gamma_{H_3}|^2} \times \left| \sum_f Q_f^2 N_C^f A_{1/2}(\tau_f) + \frac{v_{EW}}{v_R} \left( \frac{1}{3} + \frac{4}{3} - 7 \right) \right|^2. \quad (5.20)$$

where the factors of  $1/3$ ,  $4/3$  and  $-7$  are respectively from the heavy  $H_1^\pm$ ,  $H_2^{\pm\pm}$  and  $W_R$  loops in the limit of  $m_{H_3} \rightarrow 0$  [cf. Eq. (A.16)]. The current most stringent upper limits on  $\text{BR}(B_d \rightarrow \gamma\gamma)$  and  $\text{BR}(B_s \rightarrow \gamma\gamma)$  are respectively  $3.3 \times 10^{-7}$  from BaBar [76] and  $3.1 \times 10^{-6}$  from Belle [77].

Suppressed by the loop-induced  $H_3\gamma\gamma$  coupling, the limits from  $\text{BR}(B_q \rightarrow \gamma\gamma)$  are less stringent than the tree-level processes  $d_j \rightarrow d_i H_3$  discussed above. Furthermore, the FCNC effects are dominated by the  $\sin\theta_2$  couplings, thus the limits on  $\sin\theta_1$  could hardly be constrained by the diphoton decays of  $B$  mesons. The limits on  $\sin\theta_2$  are presented in Figure 6. Though  $\text{BR}(B_s \rightarrow \gamma\gamma)$  is less constrained than that of  $B_d$  meson, it is comparatively enhanced by the larger coupling of  $H_3\bar{s}b$  than  $H_3\bar{d}b$ , thus the former could exclude a larger region in Figure 6.

The bottomonium mesons  $\Upsilon$  could decays into  $\gamma H_3$  at the tree level, triggered by the flavor-conserving coupling of  $H_3$  to  $b$  quark. A light scalar has been searched for in the final state of  $\mu^+\mu^-$  [78],  $\tau^+\tau^-$  [79] and hadrons [80]. The BR can be normalized to  $\text{BR}(\Upsilon \rightarrow \mu^+\mu^-)$ , with

$$\frac{\text{BR}(\Upsilon \rightarrow \gamma H_3)}{\text{BR}(\Upsilon \rightarrow \mu^+\mu^-)_{\text{SM}}} = \frac{|\mathcal{Y}_{D,bb}|^2}{4\pi\alpha} \left( 1 - \frac{m_{H_3}^2}{m_\Upsilon^2} \right) \mathcal{F}(m_{H_3}), \quad (5.21)$$

where  $\mathcal{Y}_{D,bb}$  is the Yukawa coupling of  $H_3$  to  $b$  quark, from both the  $\sin\tilde{\theta}_1$  and  $\sin\tilde{\theta}_2$  terms, and  $\mathcal{F}(m_{H_3})$  is the QCD form factor, including relativistic corrections [39, 81]. As shown in Table 1, there is a relative minus sign between the  $\sin\tilde{\theta}_1$  and  $\sin\tilde{\theta}_2$  terms, thus for the specific well-motivated VEV ratio  $\xi = \kappa'/\kappa = m_b/m_t$  adopted throughout this paper, the two terms proportional to  $\sin\theta_1$  almost cancel with each other coincidentally,

$$\hat{Y}_{D,bb} \sin\tilde{\theta}_1 = y_b(\sin\theta_1 + \xi \sin\theta_2) = y_b \sin\theta_1 + y_t \xi^2 \sin\theta_2, \quad (5.22)$$

$$\left( V_L^\dagger \hat{Y}_U V_R \right)_{33} \sin\tilde{\theta}_2 \simeq y_t(\xi \sin\theta_1 + \sin\theta_2) = y_b \sin\theta_1 + y_t \sin\theta_2, \quad (5.23)$$

with only the contribution from mixing with the first two generations, which is suppressed by the small quark masses and CKM mixings to the 3rd generation. The  $\sin\theta_2$  terms, however, are not canceled, and the couplings of  $H_3$  to bottom quarks are dominated by the  $y_t \sin\theta_2$  term from the flavor changing part [cf. Eq. (5.23)]. For other small values of

$\xi = \kappa'/\kappa$  not necessarily equal to  $m_b/m_t$ , we will “recover” the  $y_b \sin \theta_1$  in Eqs. (5.22) and (5.23) with an  $\mathcal{O}(1)$  coefficient, while the  $y_t \sin \theta_2$  term will be affected only at the  $\xi^2$  level. Consequently in this case the constraints on  $\sin \theta_1$  is still weaker than  $\sin \theta_2$ . In this paper, we will not scan the full range of the small parameters  $\xi$  and  $\epsilon$ .

Gathering both the contributions from  $gg$  and  $q\bar{q}$ , the BR of the hadronic channel  $H_3 \rightarrow \text{hadrons}$  is generally larger than the leptonic modes, thus in Figure 6 we show only the constraint on  $\sin \theta_2$  from the hadronic decay of  $H_3$ , with the BR limits from  $1 \times 10^{-6}$  to  $8 \times 10^{-5}$  for  $H_3$  mass ranging from  $\sim 300$  MeV to  $\sim 8$  GeV. Requiring that  $H_3$  decays inside the detector with a radius of 3.5 m [63], we obtain the limits on  $\sin \theta_2$  as shown on the right panel of Figure 6. Note that the form factor in Eq. (5.21) becomes smaller when  $H_3$  is heavier, and the phase space also shrinks, thus the limit becomes less stringent for heavier  $H_3$ .

### 5.2.3 Beam-dump experiments

With a huge number of protons on target (PoT), the proton fixed target experiments, like CHARM [83], SHiP [84] and DUNE [85], provide a unique opportunity to generate a large number of LLPs, and thus, complementary constraints to the collision experiments discussed above.<sup>5</sup> In the beam dump experiments, a light  $H_3$  could be produced from  $K$  and  $B$  meson decay via  $K^+ \rightarrow \pi^+ H_3$ ,  $K_L \rightarrow \pi^0 H_3$  and  $B \rightarrow X_s H_3$ . The searches for  $e^+e^-$ ,  $\mu^+\mu^-$  and  $\gamma\gamma$  final states have been carried out at CHARM [83], but no signal event was found, which sets an upper limit of  $N_{\text{event}} < 2.3$  at the 90% C.L. on the contribution from beyond SM physics, as shown in Table 2. Following Refs. [37–39], the  $H_3$  production cross section is given by

$$\sigma_{H_3} \simeq \sigma_{pp} M_{pp} \left[ \frac{1}{2} \chi_s \text{BR}(K^+ \rightarrow \pi^+ H_3) + \frac{1}{4} \chi_s \text{BR}(K^0 \rightarrow \pi^0 H_3) + \chi_b \text{BR}(B \rightarrow X_s H_3) \right], \quad (5.24)$$

with  $\chi_s = 1/7$ ,  $\chi_b = 3 \times 10^{-8}$ ,  $\sigma_{pp}$  the proton-proton cross section and  $M_{pp}$  the average hadron multiplicity. Normalized to the neutral pion yield  $\sigma_{\pi^0} \simeq \sigma_{pp} M_{pp}/3$ , we can predict the total number of  $N_{H_3} \simeq 2.9 \times 10^{17} \sigma_{H_3}/\sigma_{\pi^0}$ . Then the number of events collected by the detector turns out to be

$$N_{\text{event}} = N_{H_3} \left( \sum_{\chi=e,\mu,\gamma} \text{BR}(H_3 \rightarrow \chi\chi) \right) \left[ \exp\left(-\frac{L\Gamma_{H_3}}{b}\right) - \exp\left(-\frac{(L+\Delta L)\Gamma_{H_3}}{b}\right) \right], \quad (5.25)$$

with  $L = 480$  m,  $\Delta L = 35$  m,  $b = E_{H_3}/m_{H_3}$  the boost factor where  $E_{H_3} \sim 10$  GeV [83]. Due to the huge number of events  $N_{H_3}$ , the mixing angles  $\sin \theta_{1,2}$  are expected to be severely constrained, which implies that the most stringent limits are from the  $\gamma\gamma$  channel, since this is the dominant decay mode of  $H_3$  for small mixing [cf. Figure 3]. Indeed, the  $\gamma\gamma$  limits from CHARM are much stronger than the meson decay limits discussed above, especially

<sup>5</sup>The muon beam dump experiment could in principle be used to produce  $H_3$  from bremsstrahlung processes [82], however, this is suppressed by the small Yukawa couplings of muon in the SM.

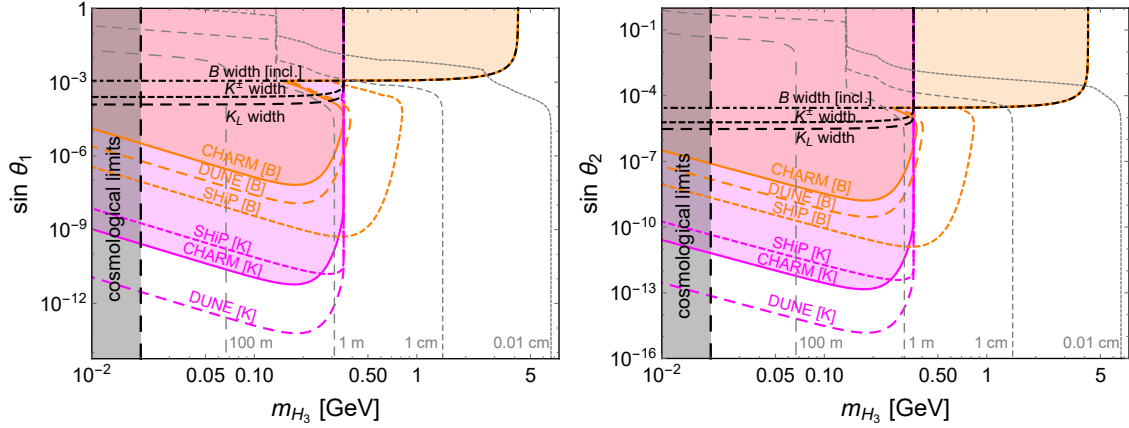


**Figure 7.** Limits on the mixing angles  $\sin \theta_{1,2}$  and  $m_{H_3}$  from the proton beam dump experiment CHARM [83] and the future prospects at SHiP [84] and DUNE [85], in the flavor-changing decays of  $K \rightarrow \pi\gamma\gamma$  and  $B \rightarrow X_s\gamma\gamma$ . For comparison, we also show the limits from the total width of  $K$  and inclusive  $B$  decays. The vertical black dashed line shows the cosmological limit. The dashed gray lines are the *proper* lifetime of  $H_3$  with values of 0.01 cm, 1 cm, 1 m, and 100 m. See text for more details.

those from the kaon decays, and could reach  $\sim 10^{-11}$  for both  $\sin \theta_1$  and  $\sin \theta_2$ , as shown in Figure 7. For lighter  $H_3$ , the boost factor  $b$  becomes larger, and fewer  $H_3$  decays inside the detector, thus the constraints get much weaker.

Regarding the future SHiP experiment [84], it is quite analogous to CHARM but with a PoT number of  $2 \times 10^{20}$ . There, we could collect  $8 \times 10^{18}$  kaon and  $7 \times 10^{13}$   $B$  meson events. With  $E_{H_3} \sim 25$  GeV,  $L = 70$  m,  $\Delta L = 55$  m and  $N_{\text{event}} < 3$ , the most stringent constraints possible are also from the  $H_3 \rightarrow \gamma\gamma$  decay mode. As shown in Figure 7, the  $K$  decay limits overlap largely with those from CHARM, while the  $B$  limits could be largely improved and broadened.

As for the DUNE experiment [85], with an even larger PoT of  $5 \times 10^{21}$ , we can collect more kaons at the near detector upstream 500 m away from the source. The total kaon number can be estimated as  $N_K \simeq N_{\text{PoT}} M_{pp} \chi_s \sim 8 \times 10^{21}$  [86] with the multiplicity  $M_{pp} = 11$  and  $\chi_s = 1/7$  for DUNE. This could largely improve the CHARM limits by about two orders of magnitude; see Figure 7. With a small  $\chi_b = 10^{-10}$  [86], the number of  $B$  mesons is much less and the expected limits from this are much weaker in Figure 7. The limits from  $D$  meson decays will be somewhat intermediate and we do not show them here.

### 5.3 SM Higgs, $Z$ and top decays

The existence of a light  $H_3$  could induce some rare or unusual decay modes for the heavier SM particles, e.g. the  $t$  quark, the Higgs and EW gauge bosons. Thus the couplings of  $H_3$  could be limited from the relevant observations of these rare decays. Firstly, the  $h - H_3$  mixing could rescale all the SM Higgs couplings universally. The current precision Higgs measurements at the LHC constrain a generic scalar mixing  $\sin \theta_1 < 0.22$  [87], which is almost a constant for  $m_{H_3} < m_h/2$ . Future more precise measurements could significantly

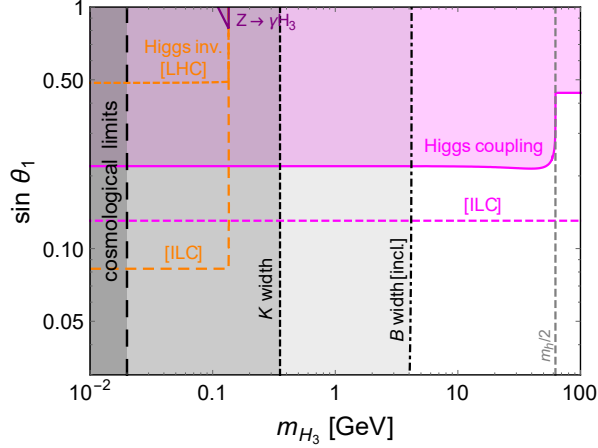


**Figure 8.** Limits on the mixing angle  $\sin \theta_1$  as a function of  $m_{H_3}$  from precision measurements at the LHC (magenta solid) [87] and future prospects at ILC (magenta dashed) [88], as well as the limits from the invisible decay of SM Higgs by the  $\sqrt{s} = 14$  TeV LHC (orange, small-dashed) [89] and  $\sqrt{s} = 1$  TeV ILC (orange, dashed) [90] data, when  $m_{H_3} < m_h/2$ . The small purple region is excluded by searches of rare  $Z \rightarrow \gamma H_3$  decay [91]. The dashed and dot-dashed black curves are the total width limit from the  $K$  and inclusive  $B$  decays. The region below 20 MeV is cosmologically disfavored. See text for more details.

improve this up to 0.13 [88]. When  $m_{H_3} < m_h/2$ , we have the extra scalar decay mode for the SM Higgs,

$$\Gamma(h \rightarrow H_3 H_3) = \frac{m_h^3 \sin^2 \theta_1}{16\pi v_R^2} \sqrt{1 - \frac{4m_{H_3}^2}{m_h^2}}. \quad (5.26)$$

If  $H_3$  is long-lived enough to escape the detector without leaving any signal, then it contributes to the invisible decay width of the SM Higgs. At the  $\sqrt{s} = 14$  TeV LHC, with an integrated luminosity of  $300 \text{ fb}^{-1}$ , the Higgs invisible BR can be constrained to be smaller than 9% at the 95% C.L. [89], while at  $\sqrt{s} = 1$  TeV ILC with a luminosity of  $1000 \text{ fb}^{-1}$ , the BR limit can reach up to 0.26% [90]. The corresponding limits on  $\sin \theta_1$  are respectively 0.49 and 0.083. The Higgs coupling and invisible decay constraints on  $\sin \theta_1$  are summarized in Figure 8, as solid/dashed magenta and orange lines respectively.

When  $m_{H_3} < m_Z$ , we have the rare  $Z$  decay  $Z \rightarrow \gamma H_3$  at one-loop level mediated by mixing with the SM Higgs, with the partial width  $\Gamma(Z \rightarrow \gamma H_3)$  given in Appendix B. With  $H_3$  decaying into two photons, we would have the three-photon final states  $Z \rightarrow \gamma H_3 \rightarrow 3\gamma$ . However, if  $m_{H_3} \ll m_Z$ , the two photons from  $H_3$  decay are highly collimated and they can not be separated experimentally. For instance, an angular separation of  $20^\circ$  requires that  $H_3$  must be above the GeV scale [91]. At LEP, the rare decay  $Z \rightarrow \gamma \pi^0$  has been performed, with an upper bound of  $5.2 \times 10^{-5}$  on the BR [92]. But this helps to constrain the mixing  $\sin \theta_1$  only by a marginal amount, as shown close to the upper border of Figure 8, because this decay into  $H_3$  arises at loop level, and we have set the decay length at 10 cm. With a huge number  $\gtrsim 10^9$  of  $Z$  events to be collected at FCC-ee [93], the limit on  $\sin \theta_1$  could be improved significantly, but it may not be able to compete with the Higgs constraints.

The flavor-changing decay of top quark into up and charm quarks, i.e.  $t \rightarrow uH_3, cH_3$  with  $H_3 \rightarrow \gamma\gamma$  could also be used to constrain the mixing angle  $\theta_1$ . Again for  $m_{H_3} \lesssim \text{GeV}$ , the photon pair can not be separated apart at the LHC, and we expect to see the signals  $t \rightarrow u\gamma, c\gamma$  with collimated photon jets. The current limit of  $1.3 \times 10^{-4}$  ( $1.7 \times 10^{-3}$ ) for  $u\gamma$  ( $c\gamma$ ) [94], can not provide any competent limits on the mixing angles  $\sin\theta_{1,2}$ , which is largely due to the small CKM mixing of the third generation with the first two in the SM.

Finally, we also note that constraints from flavor changing leptonic processes such as  $\mu \rightarrow 3e$ , are not more stringent than the hadronic decays considered above since they necessarily involve  $H_3 - H_1$  mixing as well as electron and muon Yukawa couplings, which are very small.

The most important laboratory constraints discussed in this section (i.e. those ruling out some part of the parameter space not already ruled out by others) are summarized in Figure 15, together with the collider sensitivity curves to be discussed in the next section. Here the shaded regions are all excluded. The bottom line of this summary plot is that for a GeV-scale  $H_3$  boson in the minimal LR model, the FCNC constraints necessarily imply small  $h - H_3$  and  $H_1 - H_3$  mixing angles  $\sin\theta_{1,2} \lesssim 10^{-4}$ . This naturally makes the  $H_3$  a good LLP candidate, with distinct displaced vertex signatures, as discussed below.

## 6 Production and displaced vertex searches at colliders

In this section, we discuss the production of light  $H_3$  in high-energy proton-proton collisions, and its subsequent decay to displaced photon signatures.

### 6.1 Production cross section

In the minimal LR model, the scalar  $H_3^0$  can be produced from its coupling to the heavy RH gauge bosons  $W_R$  and  $Z_R$ , as well as through its coupling to the SM Higgs [12].<sup>6</sup> For a small mixing  $\sin\theta_1 \lesssim 10^{-4}$  of our interest, which implies the scalar quartic coupling  $\alpha_1 \simeq \lambda_1 \sin\theta_1 (v_{\text{EW}}/v_R) \lesssim 10^{-6}$  [cf. Eq. (3.9)], the Higgs portal can be neglected, and we focus here only on the gauge portal production, which could be either through the heavy vector boson fusion (VBF), or associate production with a heavy vector boson (see Figure 9):

$$\begin{aligned} pp &\rightarrow W_R^* W_R^* jj \rightarrow H_3 jj, \\ pp &\rightarrow W_R^* \rightarrow W_R H_3. \end{aligned} \tag{6.1}$$

At the LHC Run II, limited by the total center-of-mass energy, the  $W_R$  production always dominates over the  $Z_R$  channel in the minimal LR scenario with  $m_{W_R} < m_{Z_R}$ , and the  $W_R H_3$  associate production cross section is smaller than that of  $W_R$  VBF, comparatively suppressed by the heavy  $W_R$  in the final state. Dictated by the gauge interaction in the RH sector, the production of  $H_3$  is only sensitive to the value of  $g_R$ , as it determines not

---

<sup>6</sup>There is also the production of  $H_3$  from photon fusion  $\gamma\gamma \rightarrow H_3$ , mediated by the  $W_R$  and scalar loops, analogous to the diagrams in Figure 2 of Ref. [95]. However, these loop-level processes turn out to be much smaller than the direct fusion of  $W_R$  and  $Z_R$  bosons in our case.

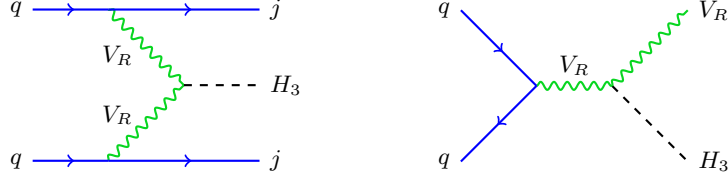


**Figure 9.** Production of  $H_3$  at hadron colliders from heavy VBF of  $W_R/Z_R$  and associate production with a heavy gauge boson  $W_R/Z_R$ .

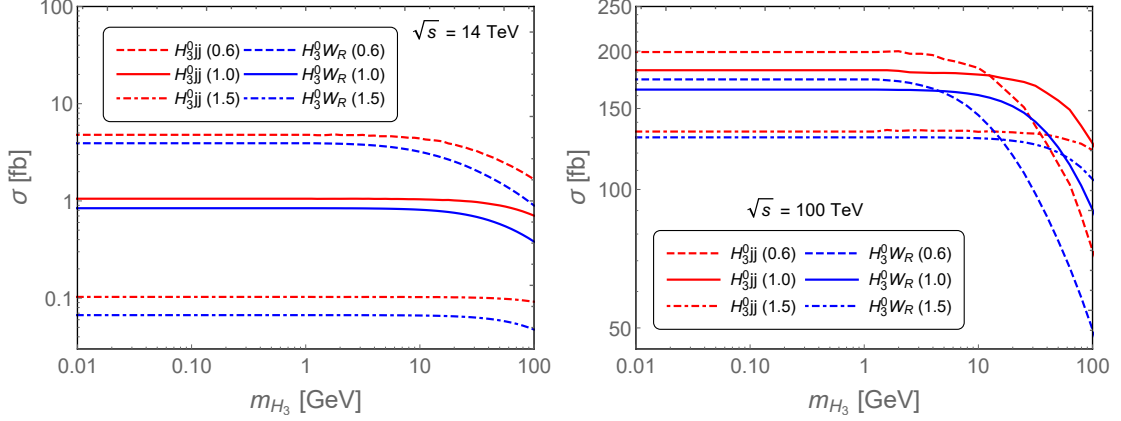


**Figure 10.** Production cross section of  $H_3^0$  at  $\sqrt{s} = 14$  TeV LHC (left) and future 100 TeV FCC-hh collider (right), as function of its mass for the heavy VBF channel  $H_3^0 jj$  and associate production  $H_3^0 W_R$ . The numbers in parentheses are the values of  $g_R/g_L$ . In both the plots we have set the RH scale  $v_R = 5$  TeV.

only the  $W_R$  mass for fixed  $v_R$  but also the magnitudes of couplings of  $W_R$  to the initial partons and  $H_3$ . The leading order production cross sections at the  $\sqrt{s} = 14$  TeV LHC for different values of  $g_R/g_L = 0.6, 1$ , and  $1.5$  are presented in the left panel of Figure 10, where we have set the RH scale  $v_R = 5$  TeV and adopted the basic trigger cuts for the VBF jets  $p_T(j) > 25$  GeV and  $\Delta\phi(jj) > 0.4$  in a MadGraph5 set up [96]. For a smaller  $g_R < g_L$ , the  $W_R$  boson is lighter and the production of  $H_3$  can be significantly enhanced. When  $m_{H_3} \lesssim 10$  GeV, the production rates are almost constant for a given  $v_R$ , and is sensitive only to the gauge coupling  $g_R$ .

## 6.2 Prospects at the LHC

Limited by the flavor constraints in Section 5, a light  $H_3$  decays mostly into two photons at the LHC after being produced and flying over a distance of  $L = bL_0$ . For a GeV mass, the decay-at-rest length  $L_0$  is of order of cm. The boost factor  $b = E_{H_3}/m_{H_3}$  depends on the distribution of energy  $E_{H_3}$  at the LHC, which is different for different values of  $g_R$ . When the gauge coupling  $g_R$  is smaller, the  $W_R$  boson is lighter and has a larger momentum, so the scalar  $H_3$  tends to be more highly boosted, with respect to the case with a heavier  $W_R$ . This effect can be seen from the energy distributions in Figure 11 from a parton-level simulation. Roughly speaking, the energy  $E_{H_3}$  has a peak at the hundred GeV scale, with

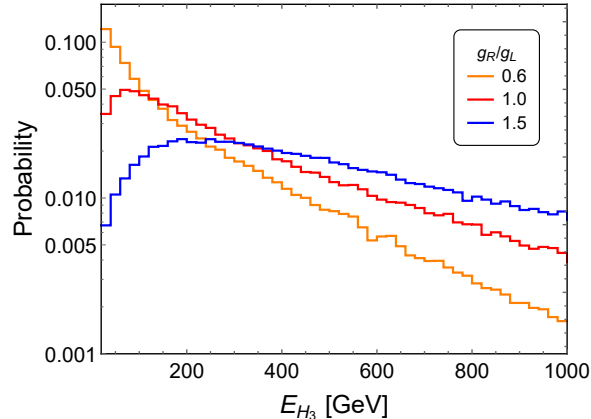


**Figure 11.** Energy distributions of the simulated events of  $H_3$  production from  $W_R$  VBF, with the probability  $(\frac{1}{\sigma} \frac{d\sigma}{dE_{H_3}}) \Delta E_{H_3}$  where  $\sigma$  is the production cross section and  $\Delta E_{H_3} = 20$  GeV is the size of the energy bins considered.

a long tail up to few TeV. For our rough sensitivity estimates, we use a boost factor of order  $\sim 100$ . Then the actual decay length is expected to be of order of meter, comparable to the radius of the Electromagnetic Calorimeter (ECAL) of ATLAS and CMS detectors, which are respectively 1.5 m [97] and 1.3 m [98, 99].

The final-state photons from  $H_3$  decay are highly collimated with a separation of  $\Delta R \sim m_{H_3}/E_{H_3}$ . Thus, in a large range of parameter space, most of the photon pairs can not be separated with the angular resolution of  $\Delta\eta \times \Delta\phi = 0.025 \times 0.025$  (ATLAS) and  $0.0174 \times 0.0174$  (CMS) [97–99], and would be identified as a high-energy single-photon jet. Counting conservatively these single photon jets within  $1 \text{ cm} < L < R_{\text{ECAL}}$ , we predict the numbers of displaced diphoton events from  $H_3$  decay in ATLAS/CMS for an integrated luminosity of  $3000 \text{ fb}^{-1}$  at  $\sqrt{s} = 14$  TeV LHC – the ultimate high-luminosity phase of LHC (HL-LHC). Our results are shown in Figure 12 for three benchmark values of  $g_R/g_L = 0.6, 1.0$  and  $1.5$  with  $v_R = 5$  TeV. Here we have applied the basic trigger cuts  $p_T(j) > 25$  GeV and  $\Delta\phi(jj) > 0.4$  on the VBF jets and have assumed the SM fake rate for the displaced diphotons to be small [100–102]. We find it promising that for a GeV-scale  $H_3$ , one could find up to  $\mathcal{O}(10^4)$  displaced photon events at the LHC, which would constitute a “smoking gun” signature of the  $H_3$  decays as predicted by the minimal LR model.

If the scalar is lighter, i.e.  $m_{H_3} \lesssim 1$  GeV, the decay length would exceed the size of LHC detectors, and could be suitable for future dedicated ultra LLP (ULLP) search experiments, such as MATHUSLA [103]. Although the surface detector MATHUSLA is much farther away from the collision point, at the 100 m scale, which provides better sensitivity for low-mass LLPs, the effective solid angle of the detector being very small, at the order of  $0.1 \times 4\pi$ , the number of events turns out to be much smaller than those at ATLAS/CMS, as shown in Figure 12 with a high luminosity of  $3000 \text{ fb}^{-1}$ . However, the background at MATHUSLA is rather low or almost negligible [103, 104], whereas the displaced photon signals at ATLAS/CMS could potentially suffer from a non-negligible background, mostly from  $\pi^0 \rightarrow \gamma\gamma$ , which has not been considered in our preliminary

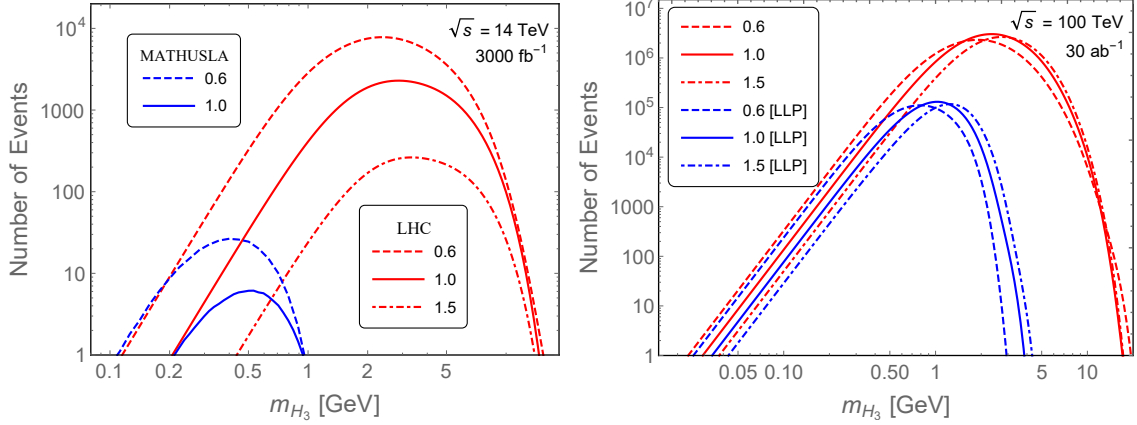


**Figure 12.** *Left:* Predicted numbers of displaced photon events from  $H_3$  decay within the ECAL of ATLAS/CMS (red) and at the proposed surface detector MATHUSLA (blue), with an integrated luminosity of  $3000 \text{ fb}^{-1}$  at  $\sqrt{s} = 14 \text{ TeV}$ , for  $g_R/g_L = 0.6, 1$  and  $1.5$ . *Right:* The corresponding numbers of displaced photon signals at FCC-hh (red) and a forward LLP detector (blue), based on a luminosity of  $30 \text{ ab}^{-1}$  at  $\sqrt{s} = 100 \text{ TeV}$ .

analysis. Thus, we believe MATHUSLA is largely complementary to the LLP searches at ATLAS/CMS, and could extend to lower mass range of  $H_3$  in the minimal LR model.

### 6.3 Prospects at future 100 TeV collider

As the physics case [105–107] for a future high-energy collider, such as FCC-hh or SPPC, with the center-of-mass energy  $\sqrt{s} = 80\text{--}100 \text{ TeV}$ , is growing rapidly, we find it worthwhile analyzing the detectable parameter space of  $H_3$  in this scenario. The production cross section are collected in the right panel of Figure 10 where for the sake of comparison we retain  $v_R = 5 \text{ TeV}$  and change only the trigger cut to  $p_T(j) > 50 \text{ GeV}$  for the VBF jets. For a light  $H_3$  with mass  $\lesssim 10 \text{ GeV}$ , the cross sections are much larger than at LHC, at the level of  $100 \text{ fb}$ , and not very sensitive to the gauge coupling  $g_R$ , as in this case the center-of-mass energy of initial partons is much larger than the  $W_R$  mass, i.e.  $\hat{s} \gg M_{W_R}$ , and the differences of cross section in Figure 10 is mainly due to the changes of couplings as we change  $g_R$ .

Given a ATLAS-like detector at FCC-hh, we predict the numbers of signal events at FCC-hh, with an integrated luminosity of  $30 \text{ ab}^{-1}$  of running at  $100 \text{ TeV}$ , which are shown by the red lines in the right panel of Figure 12. For concreteness, we assume the future detector has the same angular resolution as ATLAS, and count again only the highly collimated photon events, with a larger decay length ranging from  $L = 10 \text{ cm}$  to  $3 \text{ m}$ . With a larger cross section and higher luminosity, we can collect up to 100 times more events than at the LHC. For the LR models with a larger  $v_R$  which is beyond the scope of LHC detectability, the future higher energy colliders are the only facility to study the properties of  $H_3$ .

With a dedicated forward LLP detector at FCC-hh, similar to the one proposed in Ref. [103], the background can be significantly reduced to almost zero. With the MATH-

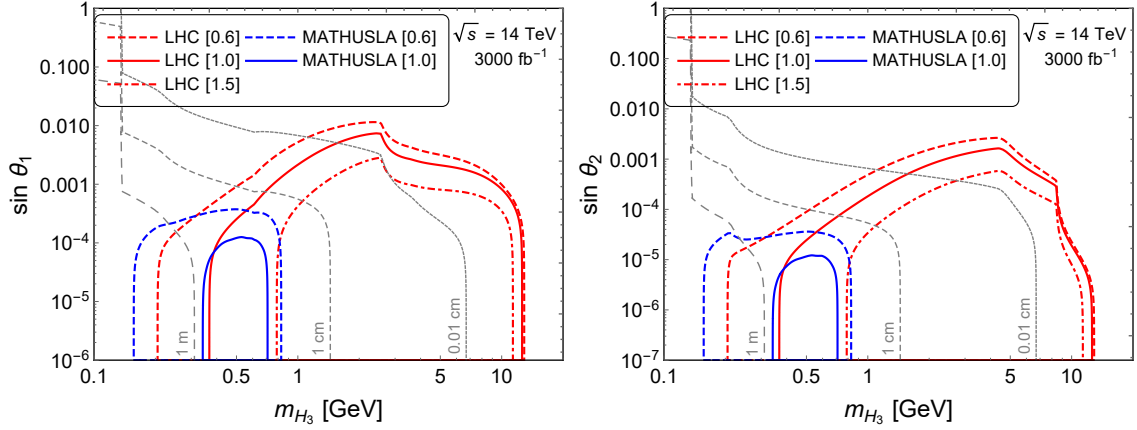


**Figure 13.** Sensitivity contours in the mass-mixing plane from future LLP searches at LHC and MATHUSLA, with an integrated luminosity of  $3000 \text{ fb}^{-1}$  running at  $\sqrt{s} = 14$  TeV, for  $g_R/g_L = 0.6, 1$  and  $1.5$ . The regions below these lines are probable with 10 signal events at LHC and 4 at MATHUSLA. The dashed gray lines are the *proper* lifetime of  $H_3$  with values of 0.01 cm, 1 cm, 1 m, and 100 m.

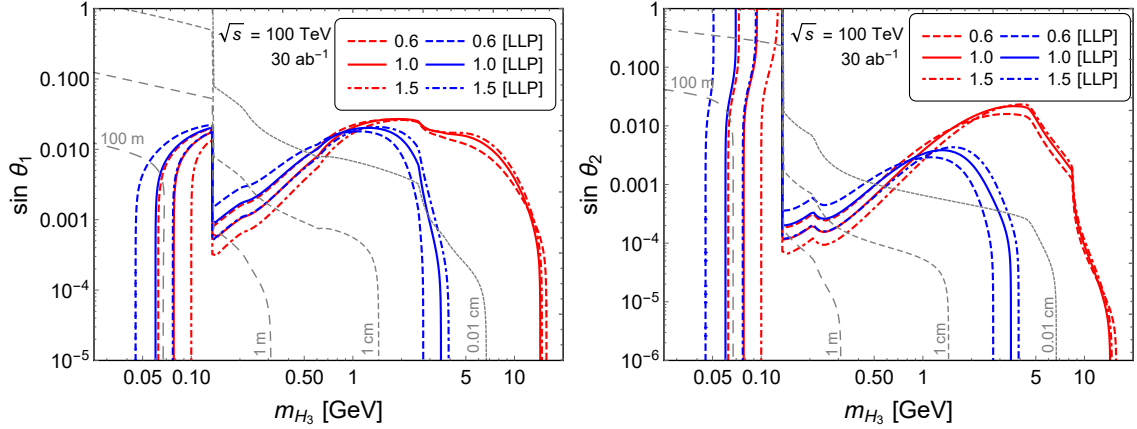


**Figure 14.** Sensitivity contours in the mass-mixing plane from future LLP searches at FCC-hh and forward LLP detector therein, with an integrated luminosity of  $30 \text{ ab}^{-1}$  running at  $\sqrt{s} = 100$  TeV, for  $g_R/g_L = 0.6, 1$  and  $1.5$ . The regions below these lines are probable with 50 signal events at FCC-hh and 10 at the forward detector. The dashed gray lines are the *proper* lifetime of  $H_3$  with values of 0.01 cm, 1 cm, 1 m, and 100 m.

USLA detector geometry as in Ref. [103], we obtain the numbers of signal events at the forward LLP detector, depicted as the blue lines in the right panel of Figure 12, for different values of  $g_R/g_L = 0.6, 1, 1.5$ .

#### 6.4 Probing the LR seesaw model

With the expected numbers of events at LHC and MATHUSLA in Figure 12, we can easily translate them to the sensitivity regions in the plane of  $m_{H_3}$  and  $\sin \theta_1$  (or  $\sin \theta_2$ ) in the LR model, assuming that the SM background for the (ultra) LLP signal is under control.



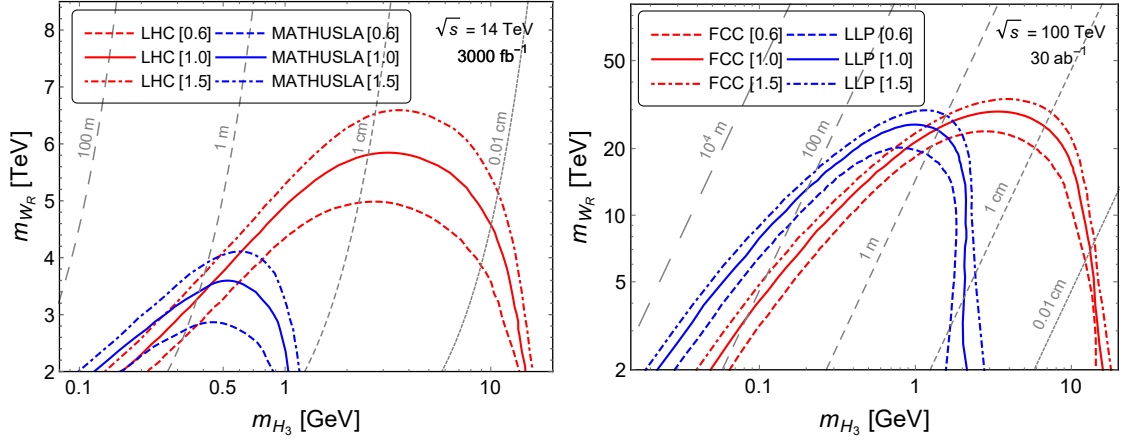


**Figure 16.** Collider sensitivity contours in the  $m_{H_3}$ - $m_{W_R}$  plane from future LLP searches at LHC and FCC-hh. The grey contours indicate the proper lifetime of  $H_3$  with  $g_R = g_L$ ; for  $g_R \neq g_L$ , the lifetime has to be rescaled by the factor of  $(g_R/g_L)^{-2}$ .

regions in the  $m_{H_3} - m_{W_R}$  plane by varying  $g_R$  and  $v_R$ , and assuming very small values of  $\sin\theta_{1,2}$  to ensure that the  $H_3 \rightarrow \gamma\gamma$  BR is almost 100%. This is shown in Figure 16 for different values of  $g_R/g_L$ . For  $g_R = g_L$ , we can probe  $m_{W_R}$  values up to 5.5 TeV or so at the LHC, which is complementary to the conventional collider searches of LR models through the same-sign dilepton plus multi-jet signal [113–126], or other collider signals in the heavy Higgs boson sector [12, 127–137].

For completeness, we also present in Appendix C an updated sensitivity study for the displaced vertex signal in the fermion sector of the LR model, namely, from light RHN decays. Again, this probes a region complementary to those being probed by the traditional collider searches [14–16].

## 7 Light neutral scalar in $U(1)_{B-L}$ model

In this section, we discuss the light neutral scalar phenomenology in a simpler model based on  $SU(2)_L \times U(1)_{I_{3R}} \times U(1)_{B-L}$  local symmetry. This  $U(1)_{B-L}$  model can be viewed in some sense as the “effective” theory of LR model at TeV scale with the  $SU(2)_R$  breaking scale and the mass of the heavy  $W_R$  bosons much higher than the TeV scale. The SM fermions are assigned to the gauge group  $SU(2)_L \times U(1)_{I_{3R}} \times U(1)_{B-L}$  as

$$\begin{aligned}
 Q &= (u_L, d_L)^T : \left( \mathbf{2}, 0, \frac{1}{3} \right); & L &= (\nu, e_L)^T : (\mathbf{2}, 0, -1); \\
 u_R &: \left( \mathbf{1}, \frac{1}{2}, \frac{1}{3} \right); & d_R &: \left( \mathbf{1}, -\frac{1}{2}, \frac{1}{3} \right); & e_R &: \left( \mathbf{1}, -\frac{1}{2}, -1 \right).
 \end{aligned} \tag{7.1}$$

Anomaly freedom requires that this model has three RHNs with gauge quantum numbers  $N_a : (\mathbf{1}, 1/2, -1)$ . The minimal Higgs fields in the model include  $H(\mathbf{2}, -1/2, 0)$  and  $\Delta(\mathbf{1}, -1, 2)$  with the following Yukawa couplings:

$$\mathcal{L}_Y = h_u \bar{Q} H u_R + h_d \bar{Q} \tilde{H} d_R + h_e \bar{L} \tilde{H} e_R + h_\nu \bar{L} H N + f \bar{N}^c \Delta N + \text{H.c.} \tag{7.2}$$

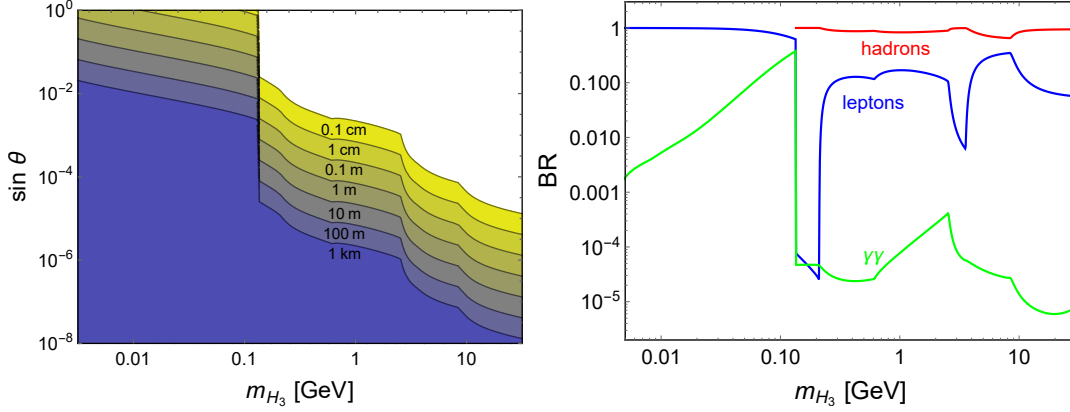


**Figure 17.** Proper lifetime and branching ratios of  $H_3$  in the  $U(1)_{B-L}$  model.

Note that  $\langle \Delta^0 \rangle = v_R$  breaks the gauge symmetry down to the SM gauge group which is further broken by  $\langle H^0 \rangle = v_{EW}$  to  $U(1)_{em}$ . From the Yukawa interactions in Eq. (7.2) it is clear that after symmetry breaking this leads to the type I seesaw formula for neutrino masses. In this model,  $H_3 = \text{Re}(\Delta^0)$ , which mixes with the SM Higgs, governed by the angle  $\sin \theta$ . Different from the LR model, in the  $U(1)_{B-L}$  model, we do not have the extra heavy gauge bosons, as well as the heavy doublet, which change essentially the production and decay properties of the light scalar  $H_3$ .

### 7.1 Couplings and decay

The couplings of  $H_3$  to the SM fermions are proportional to the SM Yukawa couplings, rescaled by the mixing angle  $\sin \theta$ , all of which are flavor conserving. However, flavor-changing coupling  $H_3 \bar{s}b$  can arise at one-loop level, through the  $W$  – top loop [108]:

$$\mathcal{L}_{\text{eff}} = \frac{3\sqrt{2}G_F m_t^2 V_{ts}^* V_{tb} \sin \theta}{16\pi^2} \frac{m_b H_3 \bar{s}_L b_R}{\sqrt{2}v_{EW}} + \text{H.c.} \quad (7.3)$$

Similarly, we can have the loop-induced flavor-changing couplings to  $ds$  and  $db$ , which are all dominated by the top-quark loops.

If  $m_{H_3} \lesssim \text{GeV}$ , it decays predominantly into the SM fermions at tree level, and into  $\gamma\gamma$  and  $gg$  at one-loop level, with the proper lifetime and branching ratios into leptons, hadrons and photons shown in Figure 4. For the hadronic modes, we combine the decays into quarks and gluons. The BRs do not depend on the mixing angle but only on  $H_3$  mass, as all the couplings are universally proportional to the mixing angle.

### 7.2 Meson limits

With the loop-level flavor-changing couplings (and tree level flavor conserving couplings), we can apply the limits from  $K$  and  $B$  meson oscillations and rare decays, as for the light scalar in the LR model (see Sections 5.1 and 5.2). Compared to the LR case, the constraints are much weaker, and the most promising limits are from the lepton ( $ee$  and  $\mu\mu$ ) and hadron decays but not the diphoton channel, which can be understood from the

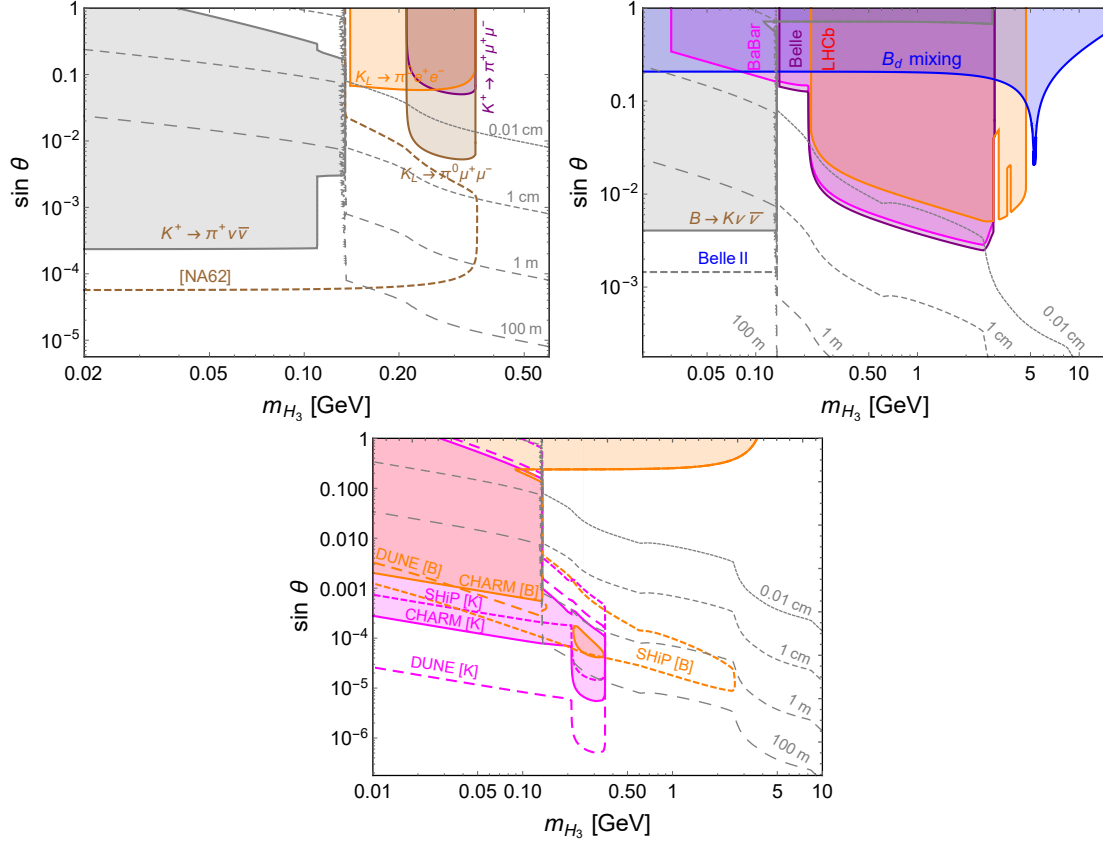


**Figure 18.** Limits on the light scalar mass  $m_{H_3}$  and its mixing with the SM Higgs  $\sin \theta$  from the  $K$  meson decay (top, left),  $B$  meson decay and oscillation (top, right) and beam-dump experiments (bottom). The  $K$  and  $B_s$  mixing limits are very weak and not shown here.

BR plot (Figure 17). All the limits on the mixing angle as a function of the  $H_3$  mass are collected in Figure 18. Note that some of the limits are very weak and not shown in the plots, such as those from the total width of  $B$  mesons, the decays  $B_s \rightarrow \mu\mu$  and  $\Upsilon \rightarrow \gamma H_3$ , and those from Higgs measurements and SM Higgs invisible decay. Nevertheless, the key feature that is common to both LR and  $U(1)_{B-L}$  models is that the meson oscillation and decay constraints rule out larger mixing angles, thus ensuring the long-lived nature of the light scalar.

### 7.3 Production and LLP searches

With the mixing angle severely constrained by the meson data, in the  $U(1)_{B-L}$  model the light scalar can only be produced from  $Z_R$  fusion, mediated by the gauge couplings. With the current LHC dilepton searches [109–112], the  $Z_R$  mass is required to be above the TeV scale. Rescaling from the  $Z'$  boson in sequential SM, we get the mass limit to be 3.72 TeV with the gauge coupling  $g_R = g_L$  in the  $U(1)_{B-L}$  model. With a smaller  $g_R = 0.825g_L$ , the constraint becomes slightly less stringent, at 3.49 TeV. The exact dependence of the production cross section (with respect to that in the sequential SM) with the ratio  $g_R/g_L$  is shown in Figure 19. With  $Z_R$  mass set at its current limit and  $g_R = g_L$  ( $g_R = 0.825g_L$ ),

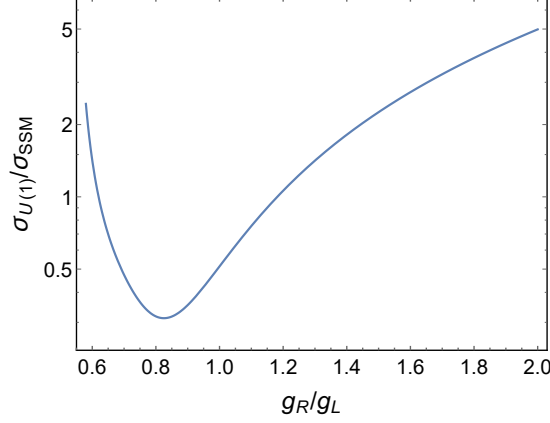


**Figure 19.** Production cross section of  $\sigma(pp \rightarrow Z_R)$  times the branching ratio into dileptons  $ee$  and  $\mu\mu$ , in units of the corresponding cross section in the sequential SM.

we obtain the production cross section of 0.31 (0.63) fb for the  $Z_R$  fusion  $pp \rightarrow Z_R^* Z_R^* jj \rightarrow H_3 jj$ .

With the coupling value  $g_R = 0.825g_L$ , which corresponds to the weakest limit on  $m_{Z'}$  from Figure 19, and therefore, the largest  $H_3$  production cross section at the LHC, we estimate the expected signal events at  $\sqrt{s} = 14$  TeV LHC with a luminosity of  $3000 \text{ fb}^{-1}$ . Assuming the signal number of 30 for the hadronic decays and 10 for the leptonic decays, we can probe a large region in the plane of  $m_{H_3}$  and  $\sin\theta$ , as shown in Figure 20. Inside the region surround by the red curve, the signal number could even reach up to few hundreds. The direct LLP searches at LHC are largely complementary to the indirect limits from meson oscillations and rare decays in Figure 18.

Limited by the  $Z_R$  mass limits and thus the production cross section, the ULLP signal number at MATHUSLA could only reach up to 2 with the detector geometry and efficiency as given in Ref. [103],<sup>7</sup> thus it is rather challenging for MATHUSLA to test the light scalar in the  $U(1)_{B-L}$  case. When  $g_R/g_L$  is different from 0.825, the  $Z'$  limits from LHC become more stringent, and it is more difficult to collect ULLP signals at MATHUSLA, irrespective of the final states being leptons or jets. However, the virtually background-free environment in the MATHUSLA detector might make it possible to probe the  $U(1)_{B-L}$  model even with such small number of signal events. The prospects at a future 100 TeV collider with a dedicated forward detector is more promising for ULLP searches.

## 8 Discussions and Conclusion

We have pointed out that, the real part of Higgs field that breaks local  $B - L$  symmetry in low-scale type I seesaw models for neutrino masses can be very light with mass in the GeV to sub-GeV range. When  $B - L$  is part of the left-right seesaw model, the light scalar couplings to Standard Model fields are so weak due to FCNC constraints on the

<sup>7</sup>We could not find any region in the plane of  $m_{H_3}$  and  $\sin\theta$  that could produce more than 4 events, which was the assumed threshold for the MATHUSLA sensitivity curves in the LR model, cf. Figure 13.

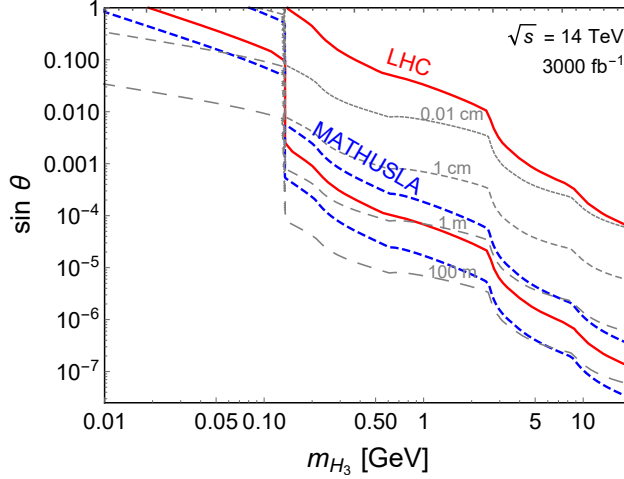


**Figure 20.** LLP search sensitivity at LHC and MATHUSLA in the  $U(1)_{B-L}$  model, with  $g_R = 0.825g_L$ . For the LHC we assume 30 signal events for the hadronic decays and 10 for the lepton final state, while for MATHUSLA we assume 2 signal events.

model that it necessarily becomes a long-lived particle, leading to high energy displaced photons at the current LHC detectors (see the summary plots in Figure 15). Searches for them could therefore provide a new probe of the TeV scale left-right seesaw models. We have also carried out an analogous discussion for the simple  $U(1)_{B-L}$  scenario. While the FCNC constraints are not so strong for this case, we show that for small mixings there can be observable displaced vertex signals (see Figure 20). We have also commented (in Appendix C) on the possibility of light right-handed neutrinos giving displaced vertices. We believe that our work provides another window in the lifetime frontier to probe the possibility of TeV scale origin of neutrino masses.

## Acknowledgments

We thank David Curtin and Brian Shuve for useful discussions and correspondence on MATHUSLA. The work of R.N.M. is supported by the US National Science Foundation grant No. PHY1620074. Y.Z. would like to thank the IISN and Belgian Science Policy (IAP VII/37) for support.

## A Partial decay widths of $H_3$

Here we collect all the partial widths for the dominant decay modes of  $H_3$ :

$$\Gamma(H_3 \rightarrow q\bar{q}) = \frac{3m_{H_3}}{16\pi} \left[ \sum_{i,j} |\mathcal{Y}_{u,ij}|^2 \beta_2^3(m_{H_3}, m_{u_i}, m_{u_j}) \Theta(m_{H_3} - m_{u_i} - m_{u_j}) + \sum_{i,j} |\mathcal{Y}_{d,ij}|^2 \beta_2^3(m_{H_3}, m_{d_i}, m_{d_j}) \Theta(m_{H_3} - m_{d_i} - m_{d_j}) \right] \quad (\text{A.1})$$

$$\Gamma(H_3 \rightarrow \ell^+ \ell^-) = \frac{m_{H_3}}{16\pi} \sum_{i,j} |\mathcal{Y}_{e,ij}|^2 \beta_2^3(m_{H_3}, m_{e_i}, m_{e_j}) \Theta(m_{H_3} - m_{e_i} - m_{e_j}), \quad (\text{A.2})$$

$$\begin{aligned} \Gamma(H_3 \rightarrow \gamma\gamma) = & \frac{\alpha^2 m_{H_3}^3}{1028\pi^3} \left| \frac{\sqrt{2}}{v_R} A_0(\tau_{H_1^\pm}) + \frac{4\sqrt{2}}{v_R} A_0(\tau_{H_2^{\pm\pm}}) \right. \\ & \left. + \frac{\sqrt{2}}{v_{\text{EW}}} \sum_{f=q,\ell} f_f N_C^f Q_f A_{1/2}(\tau_f) + \frac{\sqrt{2}}{v_R} A_1(\tau_{W_R}) \right|^2, \end{aligned} \quad (\text{A.3})$$

$$\Gamma(H_3 \rightarrow gg) = \frac{G_F \alpha_s^2 m_{H_3}^3}{36\sqrt{2}\pi^3} \left| \frac{3}{4} \sum_{f=q} f_f A_{1/2}(\tau_f) \right|^2, \quad (\text{A.4})$$

with the kinetic function

$$\beta_2(M, m_1, m_2) \equiv \left[ 1 - \frac{2(m_1^2 + m_2^2)}{M^2} + \frac{(m_1^2 - m_2^2)^2}{M^4} \right]^{1/2}, \quad (\text{A.5})$$

$\mathcal{Y}_{u,d,e}$  the Yukawa couplings given in Table 1,

$$\mathcal{Y}_u = \widehat{Y}_U \sin \tilde{\theta}_1 - (V_L \widehat{Y}_D V_R^\dagger) \sin \tilde{\theta}_2, \quad (\text{A.6})$$

$$\mathcal{Y}_d = \widehat{Y}_D \sin \tilde{\theta}_1 - (V_L^\dagger \widehat{Y}_U V_R) \sin \tilde{\theta}_2, \quad (\text{A.7})$$

$$\mathcal{Y}_e = \widehat{Y}_E \sin \tilde{\theta}_1 - Y_{\nu N} \sin \tilde{\theta}_2, \quad (\text{A.8})$$

$f_f$  the normalization factor with respect to the SM Yukawa couplings,

$$f_{u,i} = \sin \tilde{\theta}_1 - \frac{(V_L \widehat{M}_d V_R^\dagger)_{ii}}{m_{u,i}} \sin \tilde{\theta}_2, \quad (\text{A.9})$$

$$f_{d,i} = \sin \tilde{\theta}_1 - \frac{(V_L^\dagger \widehat{M}_u V_R)_{ii}}{m_{d,i}} \sin \tilde{\theta}_2, \quad (\text{A.10})$$

$$f_{e,i} = \sin \tilde{\theta}_1 - \frac{Y_{\nu N,ii}}{m_{e,i}/v_{\text{EW}}} \sin \tilde{\theta}_2, \quad (\text{A.11})$$

and the loop functions

$$A_0(\tau) \equiv -[\tau - f(\tau)] \tau^{-2}, \quad (\text{A.12})$$

$$A_{1/2}(\tau) \equiv 2[\tau + (\tau - 1)f(\tau)] \tau^{-2}, \quad (\text{A.13})$$

$$A_1(\tau) \equiv -[2\tau^2 + 3\tau + 3(2\tau - 1)f(\tau)] \tau^{-2}, \quad (\text{A.14})$$

with  $\tau_X = m_{H_3}^2/4m_X^2$  and

$$f(\tau) \equiv \begin{cases} \arcsin^2 \sqrt{\tau} & (\text{for } \tau \leq 1) \\ -\frac{1}{4} \left[ \log \left( \frac{1+\sqrt{1-1/\tau}}{1-\sqrt{1-1/\tau}} \right) - i\pi \right]^2 & (\text{for } \tau > 1). \end{cases} \quad (\text{A.15})$$

For the heavy particle loops, only the limits below are useful for us

$$A_0(0) = 1/3, \quad A_{1/2}(0) = 4/3, \quad A_1(0) = -7. \quad (\text{A.16})$$

Thus in Eq. (A.3), we have a suppression factor of  $5A_0(0)/A_1(0) = -5/21$  for scalar loops, with the factor of 5 coming from the sum of electric charges squared.

## B Rare $Z$ decay $Z \rightarrow \gamma H_3$

The partial width of rare  $Z$  decay reads

$$\Gamma(Z \rightarrow \gamma H_3) = \frac{G_F^2 \alpha m_W^2}{192 \pi^4} m_Z^3 \left(1 - \frac{m_{H_3}^2}{m_Z^2}\right)^3 \times \left| \sin \theta_1 A_1(\tau_W, \lambda_W) + \sum_{f=q,\ell} \frac{f_f N_C^f Q_f \hat{v}_f}{c_W} A_{1/2}(\tau_f, \lambda_f) \right|^2, \quad (\text{B.1})$$

with  $\tau_X = 4m_X^2/m_{H_3}^2$ ,  $\lambda_X = 4m_X^2/m_Z^2$ , and the loop functions are defined as

$$A_{1/2}(\tau, \lambda) \equiv I_1(\tau, \lambda) - I_2(\tau, \lambda), \quad (\text{B.2})$$

$$A_1(\tau, \lambda) \equiv c_W \left[ 4 \left( 3 - \frac{s_W^2}{c_W^2} \right) I_2(\tau, \lambda) + \left( \left( 1 + \frac{2}{\tau} \right) \frac{s_W^2}{c_W^2} - \left( 5 + \frac{2}{\tau} \right) \right) I_1(\tau, \lambda) \right], \quad (\text{B.3})$$

with

$$I_1(\tau, \lambda) \equiv \frac{\tau \lambda}{2(\tau - \lambda)} + \frac{\tau^2 \lambda^2}{2(\tau - \lambda)^2} [f(\tau^{-1}) - f(\lambda^{-1})] + \frac{\tau^2 \lambda}{(\tau - \lambda)^2} [g(\tau^{-1}) - g(\lambda^{-1})], \quad (\text{B.4})$$

$$I_2(\tau, \lambda) \equiv -\frac{\tau \lambda}{2(\tau - \lambda)} [f(\tau^{-1}) - f(\lambda^{-1})], \quad (\text{B.5})$$

$f(x)$  as defined in Eq. (A.15), and

$$g(\tau) \equiv \begin{cases} \frac{\sqrt{\tau^{-1} - 1} \arcsin \sqrt{\tau}}{2} & (\text{for } \tau \leq 1) \\ \frac{\sqrt{1 - \tau^{-1}}}{2} \left[ \log \left( \frac{1 + \sqrt{1 - 1/\tau}}{1 - \sqrt{1 - 1/\tau}} \right) - i\pi \right] & (\text{for } \tau > 1). \end{cases} \quad (\text{B.6})$$

## C Light RH neutrinos in the LR seesaw model

The RHNs have extra charged current interactions in the LR model mediated by the heavy  $W_R$  boson, which are not suppressed by the heavy-light neutrino mixings, but sensitive to the RH scale  $v_R$  (or equivalently the  $W_R$  mass, up to the gauge coupling  $g_R$ ). Though the ULLP signals in this case are very similar to the light scalar case discussed in Section 6.4, i.e. highly collimated leptonic and hadronic jets, the production modes and phenomenological implications are very different.

In the LR model, the decay of RHNs are predominantly mediated by an off-shell heavy  $W_R$  boson:  $N \rightarrow W_R^* \ell \rightarrow \ell jj$ . When  $m_N \ll m_{W_R}$  which is the case for a light RHN to be viable ULLP candidate at the LHC, the three-body decay width is given by

$$\Gamma_N \simeq \frac{3G_F^2}{32\pi^3} m_N^5 \left( \frac{m_W}{m_{W_R}} \frac{g_R}{g_L} \right)^4. \quad (\text{C.1})$$

For a few-TeV scale  $W_R$ , if the RHN mass is order 10 GeV, then its *proper* lifetime would be at the cm level:

$$\tau_N^0 \simeq 9.3 \times 10^{-3} \left( \frac{m_N}{10 \text{ GeV}} \right)^{-5} \left( \frac{m_{W_R}}{3 \text{ TeV}} \right)^4 \left( \frac{g_R}{g_L} \right)^{-4} \text{ m}. \quad (\text{C.2})$$

Such a light RHN at the GeV scale can be produced from rare meson decays, such as  $D_s \rightarrow eN$  (here for simplicity we assume the RHN is of electron flavor), with the subsequent decay  $N \rightarrow e\pi$  [138]. Both the production of  $N$  from mesons and decay into lighter states are mediated by its gauge interaction to the heavy  $W_R$  boson. The masses  $m_{W_R}$ ,  $m_N$  and the gauge coupling  $g_R$  can thus be probed at dedicated beam dump experiments, such as SHiP [84, 138]. Here we present a sensitivity study for the displaced vertex signal at the LHC.<sup>8</sup>

In the minimal LR model with the  $SU(2)_R$  gauge symmetry broken by the RH triplet scalar,  $m_{Z_R} > m_{W_R}$ . Thus the dominant production of RHNs at the LHC is through the  $s$ -channel  $W_R$  exchange:  $pp \rightarrow W_R^{(*)} \rightarrow \ell N$ , followed by the three-body decay  $N \rightarrow W_R^{*\ell} \rightarrow \ell jj$  [113]. With  $m_{W_R} \gtrsim 3 \text{ TeV} (g_R/g_L)^4$ , as required to satisfy the direct LHC constraints [14–16], as well as the low-energy FCNC constraints [17], the production cross section could reach few tens of fb, depending on the  $W_R$  mass as well as the gauge coupling  $g_R$ . Here we have imposed the condition that the associated lepton (jet) must satisfy the basic trigger cuts of  $p_T > 25 \text{ GeV}$  and  $|\eta| < 2.5$ . Requiring that the decay length  $1 \text{ cm} < L_N < 1.5 \text{ m}$  with the ECAL size of the ATLAS detector, we obtain the sensitivity reach for light RHN as shown in Figure 21 for three different values of the gauge coupling  $g_R/g_L = 0.6, 1$  and  $1.5$  at the  $\sqrt{s} = 14 \text{ TeV}$  HL-LHC with an integrated luminosity of  $3000 \text{ fb}^{-1}$ . For concreteness, we have assumed only the electron flavor  $\ell = e$  without RH leptonic mixing, and the number of signal events to be 10. Note that in Figure 21 even when the heavy  $W_R$  is off-shell, i.e.  $m_{W_R} \gtrsim 5 \text{ TeV}$ , the light RHN could yet be produced abundantly. For the purpose of illustration, we also show the proper lifetime of RHN for  $g_R = g_L$ , estimated from Eq. (C.2); for the values of  $g_R \neq g_L$  the lifetime should be rescaled via  $(g_R/g_L)^{-4}$  accordingly. Depending on  $g_R$ , the general-purpose detectors at LHC could probe the lifetime  $\tau_N^0$  from  $\sim 10 \text{ m}$  to below  $0.01 \text{ cm}$ , after taking into consideration the large Lorentz boost factor  $E_N/m_N$ . The RH sector can be probed up to  $m_{W_R} \simeq 20 \text{ TeV}$  for a large  $g_R/g_L = 1.5$ .

We also show the sensitivity contours for MATHUSLA in Figure 21, assuming at least 4 signal events. Though the effective cross section is smaller (due to its smaller size), MATHUSLA is sensitive to lighter RHN with mass as low as  $\sim 1 \text{ GeV}$ , and could effectively probe a complementary parameter space of LR seesaw with GeV-scale light RHNs.

## References

- [1] P. Minkowski, Phys. Lett. B **67**, 421 (1977).

<sup>8</sup>In the minimal type I seesaw model without the LR symmetry, the small Yukawa couplings of the RHNs also make them long-lived with displaced vertex signatures at colliders [139, 140]; however, their production cross section will also be suppressed by the same Yukawa couplings.

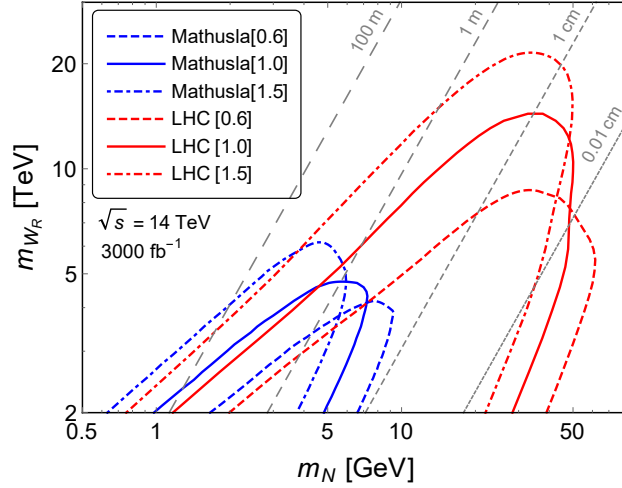


**Figure 21.** Light RHN sensitivity in the minimal LR model from the ULLP searches at the  $\sqrt{s} = 14$  TeV LHC (red) and MATHUSLA (blue) for three different values of  $g_R/g_L = 0.6, 1$  and  $1.5$ . The grey contours indicate the proper decay length of RHN with  $g_R = g_L$ ; for  $g_R \neq g_L$ , the lifetime has to be rescaled by the factor of  $(g_R/g_L)^{-4}$ .

- [2] R. N. Mohapatra and G. Senjanović, Phys. Rev. Lett. **44**, 912 (1980).
- [3] T. Yanagida, Conf. Proc. C **7902131**, 95 (1979).
- [4] M. Gell-Mann, P. Ramond and R. Slansky, Conf. Proc. C **790927**, 315 (1979) [arXiv:1306.4669 [hep-th]].
- [5] S. L. Glashow, NATO Sci. Ser. B **61**, 687 (1980).
- [6] J. C. Pati and A. Salam, Phys. Rev. D **10**, 275 (1974).
- [7] R. N. Mohapatra and J. C. Pati, Phys. Rev. D **11** 2558 (1975).
- [8] G. Senjanović and R. N. Mohapatra, Phys. Rev. D **12** 1502 (1975).
- [9] P. S. B. Dev, R. N. Mohapatra and Y. Zhang, arXiv:1612.09587 [hep-ph].
- [10] D. Chang, R. N. Mohapatra and M. K. Parida, Phys. Rev. Lett. **52**, 1072 (1984).
- [11] N. G. Deshpande, J. F. Gunion, B. Kayser and F. I. Olness, Phys. Rev. D **44**, 837 (1991).
- [12] P. S. B. Dev, R. N. Mohapatra and Y. Zhang, JHEP **1605**, 174 (2016) [arXiv:1602.05947 [hep-ph]].
- [13] A. Maiezza, G. Senjanović and J. C. Vasquez, arXiv:1612.09146 [hep-ph].
- [14] V. Khachatryan *et al.* [CMS Collaboration], Eur. Phys. J. C **74**, 3149 (2014) [arXiv:1407.3683 [hep-ex]].
- [15] G. Aad *et al.* [ATLAS Collaboration], JHEP **1507**, 162 (2015) [arXiv:1506.06020 [hep-ex]].
- [16] V. Khachatryan *et al.* [CMS Collaboration], arXiv:1612.01190 [hep-ex].
- [17] S. Bertolini, A. Maiezza and F. Nesti, Phys. Rev. D **89**, no. 9, 095028 (2014) [arXiv:1403.7112 [hep-ph]].
- [18] I. Z. Rothstein, Nucl. Phys. B **358**, 181 (1991).
- [19] R. Kuchimanchi, Phys. Rev. D **91**, no. 7, 071901 (2015) [arXiv:1408.6382 [hep-ph]].

- [20] J. Chakraborty, J. Gluza, T. Jelinski and T. Srivastava, Phys. Lett. B **759**, 361 (2016) [arXiv:1604.06987 [hep-ph]].
- [21] A. Maiezza, M. Nemevšek and F. Nesti, Phys. Rev. D **94**, no. 3, 035008 (2016) [arXiv:1603.00360 [hep-ph]].
- [22] S. R. Coleman and E. J. Weinberg, Phys. Rev. D **7**, 1888 (1973).
- [23] A. D. Linde, JETP Lett. **23**, 64 (1976).
- [24] S. Weinberg, Phys. Rev. Lett. **36**, 294 (1976).
- [25] M. Holthausen, M. Lindner and M. A. Schmidt, Phys. Rev. D **82**, 055002 (2010) [arXiv:0911.0710 [hep-ph]].
- [26] J. A. Casas and A. Ibarra, Nucl. Phys. B **618**, 171 (2001) [hep-ph/0103065].
- [27] P. S. B. Dev, R. N. Mohapatra and Y. Zhang, JHEP **1602**, 186 (2016) [arXiv:1512.08507 [hep-ph]].
- [28] G. Senjanović and V. Tello, Phys. Rev. Lett. **114**, no. 7, 071801 (2015) [arXiv:1408.3835 [hep-ph]].
- [29] G. Senjanović and V. Tello, Phys. Rev. D **94**, no. 9, 095023 (2016) [arXiv:1502.05704 [hep-ph]].
- [30] P. A. R. Ade *et al.* [Planck Collaboration], Astron. Astrophys. **594**, A13 (2016) [arXiv:1502.01589 [astro-ph.CO]].
- [31] Y. Zhang, H. An, X. Ji and R. N. Mohapatra, Nucl. Phys. B **802**, 247 (2008) [arXiv:0712.4218 [hep-ph]].
- [32] R. Babich, N. Garron, C. Hoelbling, J. Howard, L. Lellouch and C. Rebbi, Phys. Rev. D **74**, 073009 (2006) [hep-lat/0605016].
- [33] A. J. Buras, S. Jager and J. Urban, Nucl. Phys. B **605**, 600 (2001) [hep-ph/0102316].
- [34] C. Patrignani *et al.* (Particle Data Group), Chin. Phys. C, **40**, 100001 (2016).
- [35] D. Becirevic, V. Gimenez, G. Martinelli, M. Papinutto and J. Reyes, JHEP **0204** (2002) 025 [hep-lat/0110091].
- [36] J. Charles *et al.*, Phys. Rev. D **91**, no. 7, 073007 (2015) [arXiv:1501.05013 [hep-ph]].
- [37] F. Bezrukov and D. Gorbunov, JHEP **1005**, 010 (2010) [arXiv:0912.0390 [hep-ph]].
- [38] J. D. Clarke, R. Foot and R. R. Volkas, JHEP **1402**, 123 (2014) [arXiv:1310.8042 [hep-ph]].
- [39] M. J. Dolan, F. Kahlhoefer, C. McCabe and K. Schmidt-Hoberg, JHEP **1503**, 171 (2015) Erratum: [JHEP **1507**, 103 (2015)] [arXiv:1412.5174 [hep-ph]].
- [40] E. Izaguirre, T. Lin and B. Shuve, arXiv:1611.09355 [hep-ph].
- [41] X. G. He, J. Tandean and G. Valencia, Phys. Rev. D **74**, 115015 (2006) [hep-ph/0610274].
- [42] A. Z. Dubnickova, S. Dubnicka, E. Goudzovski, V. N. Pervushin and M. Secansky, Phys. Part. Nucl. Lett. **5**, 76 (2008) [hep-ph/0611175].
- [43] J. R. Batley *et al.* [NA48/2 Collaboration], Phys. Lett. B **677**, 246 (2009) [arXiv:0903.3130 [hep-ex]].
- [44] J. R. Batley *et al.* [NA48/2 Collaboration], Phys. Lett. B **697**, 107 (2011) [arXiv:1011.4817 [hep-ex]].

- [45] J. M. Gerard, C. Smith and S. Trine, Nucl. Phys. B **730**, 1 (2005) [hep-ph/0508189].
- [46] C. Lazzeroni *et al.* [NA62 Collaboration], Phys. Lett. B **732**, 65 (2014) [arXiv:1402.4334 [hep-ex]].
- [47] V. V. Anisimovsky *et al.* [E949 Collaboration], Phys. Rev. Lett. **93**, 031801 (2004) [hep-ex/0403036].
- [48] A. V. Artamonov *et al.* [E949 Collaboration], Phys. Rev. Lett. **101**, 191802 (2008) [arXiv:0808.2459 [hep-ex]].
- [49] A. V. Artamonov *et al.* [BNL-E949 Collaboration], Phys. Rev. D **79**, 092004 (2009) [arXiv:0903.0030 [hep-ex]].
- [50] A. V. Artamonov *et al.* [E949 Collaboration], Phys. Rev. D **72**, 091102 (2005) [hep-ex/0506028].
- [51] S. Adler *et al.* [E949 and E787 Collaborations], Phys. Rev. D **77**, 052003 (2008) [arXiv:0709.1000 [hep-ex]].
- [52] G. Anelli *et al.*, CERN-SPSC-2005-013, CERN-SPSC-P-326.
- [53] A. J. Buras, D. Buttazzo, J. Girrbach-Noe and R. Knegjens, JHEP **1511**, 033 (2015) [arXiv:1503.02693 [hep-ph]].
- [54] A. Alavi-Harati *et al.* [KTeV Collaboration], Phys. Rev. Lett. **93**, 021805 (2004) [hep-ex/0309072].
- [55] A. Alavi-Harati *et al.* [KTEV Collaboration], Phys. Rev. Lett. **84**, 5279 (2000) [hep-ex/0001006].
- [56] E. Abouzaid *et al.* [KTeV Collaboration], Phys. Rev. D **77**, 112004 (2008) [arXiv:0805.0031 [hep-ex]].
- [57] T. Alexopoulos *et al.* [KTeV Collaboration], Phys. Rev. D **70**, 092006 (2004) [hep-ex/0406002].
- [58] P. Ball and R. Zwicky, Phys. Rev. D **71**, 014015 (2005) [hep-ph/0406232].
- [59] A. Ali, P. Ball, L. T. Handoko and G. Hiller, Phys. Rev. D **61**, 074024 (2000) [hep-ph/9910221].
- [60] B. Aubert *et al.* [BaBar Collaboration], Phys. Rev. Lett. **91**, 221802 (2003) [hep-ex/0308042].
- [61] J.-T. Wei *et al.* [Belle Collaboration], Phys. Rev. Lett. **103**, 171801 (2009) [arXiv:0904.0770 [hep-ex]].
- [62] R. Aaij *et al.* [LHCb Collaboration], JHEP **1302**, 105 (2013) [arXiv:1209.4284 [hep-ex]].
- [63] B. Aubert *et al.* [BaBar Collaboration], Nucl. Instrum. Meth. A **479**, 1 (2002) [hep-ex/0105044].
- [64] T. Abe *et al.* [Belle-II Collaboration], arXiv:1011.0352 [physics.ins-det].
- [65] A. A. Alves, Jr. *et al.* [LHCb Collaboration], JINST **3**, S08005 (2008).
- [66] R. Ammar *et al.* [CLEO Collaboration], Phys. Rev. Lett. **87**, 271801 (2001) [hep-ex/0106038].
- [67] J. P. Lees *et al.* [BaBar Collaboration], Phys. Rev. D **87**, no. 11, 112005 (2013) [arXiv:1303.7465 [hep-ex]].

- [68] W. Altmannshofer, A. J. Buras, D. M. Straub and M. Wick, JHEP **0904**, 022 (2009) [arXiv:0902.0160 [hep-ph]].
- [69] W. Altmannshofer, P. Paradisi and D. M. Straub, JHEP **1204**, 008 (2012) [arXiv:1111.1257 [hep-ph]].
- [70] <http://lhcb-public.web.cern.ch/lhcb-public/>
- [71] R. Aaij *et al.* [LHCb Collaboration], Phys. Rev. Lett. **111**, 101805 (2013) [arXiv:1307.5024 [hep-ex]].
- [72] S. Chatrchyan *et al.* [CMS Collaboration], Phys. Rev. Lett. **111**, 101804 (2013) [arXiv:1307.5025 [hep-ex]].
- [73] CMS and LHCb Collaborations [CMS and LHCb Collaborations], CMS-PAS-BPH-13-007, LHCb-CONF-2013-012, CERN-LHCb-CONF-2013-012.
- [74] J. I. Aranda, A. Flores-Tlalpa, F. Ramirez-Zavaleta, F. J. Tlachino, J. J. Toscano and E. S. Tututi, Phys. Rev. D **79**, 093009 (2009) [arXiv:0905.4767 [hep-ph]].
- [75] J. I. Aranda, J. Montano, F. Ramirez-Zavaleta, J. J. Toscano and E. S. Tututi, Phys. Rev. D **82**, 054002 (2010) [arXiv:1005.5452 [hep-ph]].
- [76] P. del Amo Sanchez *et al.* [BaBar Collaboration], Phys. Rev. D **83**, 032006 (2011) [arXiv:1010.2229 [hep-ex]].
- [77] D. Dutta *et al.* [Belle Collaboration], Phys. Rev. D **91**, no. 1, 011101 (2015) [arXiv:1411.7771 [hep-ex]].
- [78] J. P. Lees *et al.* [BaBar Collaboration], Phys. Rev. D **87**, no. 3, 031102 (2013) Erratum: [Phys. Rev. D **87**, no. 5, 059903 (2013)] [arXiv:1210.0287 [hep-ex]].
- [79] J. P. Lees *et al.* [BaBar Collaboration], Phys. Rev. D **88**, no. 7, 071102 (2013) [arXiv:1210.5669 [hep-ex]].
- [80] J. P. Lees *et al.* [BaBar Collaboration], Phys. Rev. Lett. **107**, 221803 (2011) [arXiv:1108.3549 [hep-ex]].
- [81] F. Wilczek, Phys. Rev. Lett. **39**, 1304 (1977).
- [82] C. Y. Chen, M. Pospelov and Y. M. Zhong, arXiv:1701.07437 [hep-ph].
- [83] F. Bergsma *et al.* [CHARM Collaboration], Phys. Lett. **157B**, 458 (1985).
- [84] S. Alekhin *et al.*, Rept. Prog. Phys. **79**, no. 12, 124201 (2016) [arXiv:1504.04855 [hep-ph]].
- [85] C. Adams *et al.* [LBNE Collaboration], arXiv:1307.7335 [hep-ex].
- [86] D. Gorbunov and M. Shaposhnikov, JHEP **0710**, 015 (2007) Erratum: [JHEP **1311**, 101 (2013)] [arXiv:0705.1729 [hep-ph]].
- [87] A. Falkowski, C. Gross and O. Lebedev, JHEP **1505**, 057 (2015) [arXiv:1502.01361 [hep-ph]].
- [88] S. Profumo, M. J. Ramsey-Musolf, C. L. Wainwright and P. Winslow, Phys. Rev. D **91**, no. 3, 035018 (2015) [arXiv:1407.5342 [hep-ph]].
- [89] M. E. Peskin, arXiv:1207.2516 [hep-ph].
- [90] H. Baer *et al.*, arXiv:1306.6352 [hep-ph].
- [91] J. Jaeckel and M. Spannowsky, Phys. Lett. B **753**, 482 (2016) [arXiv:1509.00476 [hep-ph]].
- [92] M. Acciarri *et al.* [L3 Collaboration], Phys. Lett. B **353**, 136 (1995).

- [93] M. Bicer *et al.* [TLEP Design Study Working Group], JHEP **1401**, 164 (2014) [arXiv:1308.6176 [hep-ex]].
- [94] V. Khachatryan *et al.* [CMS Collaboration], JHEP **1604**, 035 (2016) [arXiv:1511.03951 [hep-ex]].
- [95] K. S. Babu and S. Jana, arXiv:1612.09224 [hep-ph].
- [96] J. Alwall *et al.*, JHEP **1407**, 079 (2014) [arXiv:1405.0301 [hep-ph]].
- [97] G. Aad *et al.* [ATLAS Collaboration], arXiv:0901.0512 [hep-ex].
- [98] G. L. Bayatian *et al.* [CMS Collaboration], J. Phys. G **34**, 995 (2007).
- [99] S. Chatrchyan *et al.* [CMS Collaboration], JINST **3**, S08004 (2008).
- [100] B. Dasgupta, J. Kopp and P. Schwaller, Eur. Phys. J. C **76**, no. 5, 277 (2016) [arXiv:1602.04692 [hep-ph]].
- [101] Y. Tsai, L. T. Wang and Y. Zhao, arXiv:1603.00024 [hep-ph].
- [102] H. Fukuda, M. Ibe, O. Jinnouchi and M. Nojiri, arXiv:1607.01936 [hep-ph].
- [103] J. P. Chou, D. Curtin and H. J. Lubatti, arXiv:1606.06298 [hep-ph].
- [104] A. Coccaro, D. Curtin, H. J. Lubatti, H. Russell and J. Shelton, arXiv:1605.02742 [hep-ph].
- [105] N. Arkani-Hamed, T. Han, M. Mangano and L. T. Wang, Phys. Rept. **652**, 1 (2016) [arXiv:1511.06495 [hep-ph]].
- [106] T. Golling *et al.*, arXiv:1606.00947 [hep-ph].
- [107] R. Contino *et al.*, arXiv:1606.09408 [hep-ph].
- [108] B. Batell, M. Pospelov and A. Ritz, Phys. Rev. D **83**, 054005 (2011) [arXiv:0911.4938 [hep-ph]].
- [109] The ATLAS collaboration [ATLAS Collaboration], ATLAS-CONF-2016-045.
- [110] CMS Collaboration [CMS Collaboration], CMS-PAS-EXO-16-031.
- [111] S. Patra, F. S. Queiroz and W. Rodejohann, Phys. Lett. B **752**, 186 (2016) [arXiv:1506.03456 [hep-ph]].
- [112] M. Lindner, F. S. Queiroz and W. Rodejohann, Phys. Lett. B **762**, 190 (2016) [arXiv:1604.07419 [hep-ph]].
- [113] W. Y. Keung and G. Senjanović, Phys. Rev. Lett. **50**, 1427 (1983).
- [114] A. Ferrari *et al.*, Phys. Rev. D **62**, 013001 (2000).
- [115] M. Nemevsek, F. Nesti, G. Senjanovic and Yue Zhang, Phys. Rev. D **83**, 115014 (2011) [arXiv:1103.1627 [hep-ph]].
- [116] S. P. Das, F. F. Deppisch, O. Kittel and J. W. F. Valle, Phys. Rev. D **86**, 055006 (2012) [arXiv:1206.0256 [hep-ph]].
- [117] J. A. Aguilar-Saavedra and F. R. Joaquim, Phys. Rev. D **86**, 073005 (2012) [arXiv:1207.4193 [hep-ph]].
- [118] C. Y. Chen, P. S. B. Dev and R. N. Mohapatra, Phys. Rev. D **88**, 033014 (2013) [arXiv:1306.2342 [hep-ph]].
- [119] F. F. Deppisch, P. S. B. Dev and A. Pilaftsis, New J. Phys. **17**, 075019 (2015) [arXiv:1502.06541 [hep-ph]].

- [120] J. Gluza and T. Jeliński, Phys. Lett. B **748**, 125 (2015) [arXiv:1504.05568 [hep-ph]].
- [121] J. N. Ng, A. de la Puente and B. W. P. Pan, JHEP **1512**, 172 (2015) [arXiv:1505.01934 [hep-ph]].
- [122] P. S. B. Dev, D. Kim and R. N. Mohapatra, JHEP **1601**, 118 (2016) [arXiv:1510.04328 [hep-ph]].
- [123] J. Gluza, T. Jelinski and R. Szafron, Phys. Rev. D **93**, no. 11, 113017 (2016) [arXiv:1604.01388 [hep-ph]].
- [124] M. Lindner, F. S. Queiroz, W. Rodejohann and C. E. Yaguna, JHEP **1606**, 140 (2016) [arXiv:1604.08596 [hep-ph]].
- [125] M. Mitra, R. Ruiz, D. J. Scott and M. Spannowsky, Phys. Rev. D **94**, 095016 (2016) [arXiv:1607.03504 [hep-ph]].
- [126] S. S. Biswal and P. S. B. Dev, arXiv:1701.08751 [hep-ph].
- [127] J. F. Gunion, B. Kayser, R. N. Mohapatra, N. G. Deshpande, J. Grifols, A. Mendez, F. I. Olness and P. B. Pal, PRINT-86-1324 (UC,DAVIS).
- [128] G. Azuelos, K. Benslama and J. Ferland, J. Phys. G **32**, no. 2, 73 (2006) [hep-ph/0503096].
- [129] D. W. Jung and K. Y. Lee, Phys. Rev. D **78**, 015022 (2008) [arXiv:0802.1572 [hep-ph]].
- [130] P. Fileviez Perez, T. Han, G. y. Huang, T. Li and K. Wang, Phys. Rev. D **78**, 015018 (2008) [arXiv:0805.3536 [hep-ph]].
- [131] G. Bambhaniya, J. Chakraborty, J. Gluza, M. Kordiaczyska and R. Szafron, JHEP **1405**, 033 (2014) [arXiv:1311.4144 [hep-ph]].
- [132] B. Dutta, R. Eusebi, Y. Gao, T. Ghosh and T. Kamon, Phys. Rev. D **90**, 055015 (2014) [arXiv:1404.0685 [hep-ph]].
- [133] G. Bambhaniya, J. Chakraborty, J. Gluza, T. Jelinski and M. Kordiaczynska, Phys. Rev. D **90**, no. 9, 095003 (2014) [arXiv:1408.0774 [hep-ph]].
- [134] A. Maiezza, M. Nemevsek and F. Nesti, Phys. Rev. Lett. **115**, 081802 (2015) [arXiv:1503.06834 [hep-ph]].
- [135] G. Bambhaniya, J. Chakraborty, J. Gluza, T. Jelinski and R. Szafron, Phys. Rev. D **92**, no. 1, 015016 (2015) [arXiv:1504.03999 [hep-ph]].
- [136] M. Nemevsek, F. Nesti and J. C. Vasquez, arXiv:1612.06840 [hep-ph].
- [137] CMS Collaboration [CMS Collaboration], CMS-PAS-HIG-16-036.
- [138] O. Castillo-Felisola, C. O. Dib, J. C. Helo, S. G. Kovalenko and S. E. Ortiz, Phys. Rev. D **92**, no. 1, 013001 (2015) [arXiv:1504.02489 [hep-ph]].
- [139] J. C. Helo, M. Hirsch and S. Kovalenko, Phys. Rev. D **89**, 073005 (2014) Erratum: [Phys. Rev. D **93**, no. 9, 099902 (2016)] [arXiv:1312.2900 [hep-ph]].
- [140] S. Antusch, E. Cazzato and O. Fischer, JHEP **1612**, 007 (2016) [arXiv:1604.02420 [hep-ph]].